15020

学位論文

Fluorescent Indicators for Visualizing Cyclic GMP and Protein Phosphorylation in Living Cells

サイクリックGMP及び蛋白質リン酸化に基づく細胞内情報伝達を可視化する蛍光プローブ分子

平成13年1月博士（理学）申請

東京大学大学院理学系研究科化学専攻

佐藤守俊

Fluorescent Indicators for Visualizing Cyclic GMP and Protein Phosphorylation in Living Cells

A dissertation submitted to The University of Tokyo
for the degree of Doctor of Science

by **Moritoshi SATO**

Department of chemistry
The University of Tokyo

Table of Contents

Acknowledgments

This thesis is an assembly of results of my research at the Department of Chemistry, Graduate School of Science, The University of Tokyo, under the supervision of Professor Yoshio Umezawa.

I wish to express my sincere gratitude to Prof. Yoshio Umezawa for his continuous guidance, support, advice and encouragement throughout the present study.

I would like to express my deep gratitude to Dr. Takeaki Ozawa, Graduate School of Science, The University of Tokyo, for his continuous direction, advice and encouragement, and for his stimulating discussion.

I very much thank Dr. Tomoichiro Asano and Dr. Kouichi Inukai, Graduate School of Medicine, The University of Tokyo, for considerable support in experimental techniques and continuous stimulating discussion.

My special thanks are due to Mr. Naoki Hida and Mr. Taishi Yoshida, Graduate School of Science, The University of Tokyo, for considerable support in experiment, their continuous stimulating discussion and cooperative works not involved in this thesis.

My gratitude is due to Mr. Hiroshi Aoki, Mr. Jun Nakanishi, and Miss Yukiko Nishimura, Graduate School of Science, The University of Tokyo, for their stimulating discussion and continuous encouragement.

I would like to express my deep gratitude to every member of Prof. Umezawa's lab. for his/her kept helpful and stimulating atmosphere.

I would like to acknowledge the financial support by the Japan Society for the Promotion of Science (JSPS).

Finally, this thesis is dedicated to my family and my friends, for their devoted care and help to accomplish this science, and also to my 27 years and to my future.

Chapter 1.

General Introduction

1-1. Fluorescence imaging

Breakthrough for understanding signal transduction, especially in complex tissues such as those found in the central nervous system, depends on decoding the spatial localization and temporal dynamics of intra- and extracellular signaling biomolecules[1-4]. The most generally applicable and popular techniques with a high spatial and temporal resolution are optical techniques[5]. Thus, fluorescent indicators that report local concentrations of the signaling biomolecules of interest by alternations in the amplitude or wavelength distribution of their excitation or emission spectra, have been developed for several small biomolecules and ions[6, 7]. For instance, fluorescent Ca^{2+} indicators including Fura-2, Indo-1 and Quin-2 have contributed to reveal intracellular dynamics of Ca^{2+}, such as Ca^{2+} waves and Ca^{2+} oscillations, with a fluorescence microscope[6]. Also, fluorescent indicators have recently been developed for other ions and small biomolecules such as Zn^{2+}[8, 9], cyclic AMP (cAMP)[10, 11] and nitric oxide[12, 13]. Concerning with signaling proteins, green fluorescent protein (GFP) derived from the jellyfish *Aequorea* have recently been used for labeling the signaling proteins, instead of conventional synthetic dyes such as fluorescein and rhodamine, which have facilitated direct observation of the signaling proteins not only in living cells but also in tissues and organs from transgenic animals expressing fusion proteins of GFP and the signaling proteins of

interest[14, 15]. So far, fluorescence imaging is however limited to visualize several small biomolecules, ions and translocation of signaling proteins within cells. The development of fluorescent indicators for pivotal small biomolecules and protein-based signal transduction such as protein phosphorylation, acetylation, protein–protein interaction and enzymatic activation followed by conformational changes in signaling proteins, should be an active area of interest.

1-2. Purpose of the present study

I herein describe fluorescent indicators for cyclic GMP (cGMP), which is one of the major second messengers including Ca^{2+} and cAMP, and for visualizing protein phosphorylation-based signal transduction, which is one of the most pivotal mechanism for protein-based signaling, in living cells. Fluorescent indicators for cGMP, named CGYs, were developed on the basis of a genetic approach. Using CGYs, I have demonstrated that cellular accumulation of cGMP was not necessarily in parallel with agonist concentrations, and have found an oscillating dynamics of cGMP concentration in single living cells. Fluorescent indicators for observing protein phosphorylation-based signal transduction, named FRET pair and phocuses, were developed on the basis of synthetic and genetic approaches, respectively. In the present study, FRET pair and phocuses were exemplified using insulin signaling proteins, with which protein phosphorylation by insulin receptor was visualized. The present fluorescent indicators opens a way not only for understanding the dynamics of cGMP- and protein phosphorylation-based signal transduction in single live cells and organisms but also for high-throughput screening[16, 17] of pharmaceuticals from thousands of candidate chemicals.

References

1. Pawson, T. Protein modules and signaling networks. *Nature* **373**, 573-580 (1995).
2. Rosen, D.M. Localization of protein kinases by anchoring proteins: A theme in signal transduction. *Science* **268**, 247-251 (1995).
3. Pawson, T. & Scott, J.D. Signaling through scaffold, anchoring, and adaptor proteins. *Science* **278**, 2075-2080 (1997).
4. Hunter, T. Signaling—2000 and beyond. *Cell* **100**, 113-127 (2000).
5. Weiss, S. Fluorescence Spectroscopy of single biomolecules. *Science* **283**, 1676-1683 (1999).
6. Tsien, R.Y. Fluorescence imaging creates a window on the cell. *Chemical and engineering news* **July 18**, 34-44 (1994).
7. Zacharias, D.A., Baird, G.S. & Tsien, R.Y. Recent advances in technology for measuring and manipulating cell signals. *Curr. Opinion Neurobiol.* **10**, 416-421 (2000).
8. Czarnik, A.W. Principles of fluorescent probe design for ion recognition. *Topics in fluorescence spectroscopy* **4**, 49-70 (1994).
9. Walkup, G.K. & Imperiali, B. Fluorescent chemosensors for divalent zinc based on zinc finger domains. Enhanced oxidative stability, metal binding affinity, and structual and functional characterization. *J. Am. Chem. Soc* **119**, 3443-3450 (1997).
10. Adams, S.R., Harootunian, A.T., Buechler, Y.J., Taylor, S.S. & Tsien, R.Y. Fluorescence ratio imaging of cyclic AMP in single cells. *Nature* **349**, 694-697 (1991).

11. Zaccolo, M., *et al.* A genetically encoded, fluorescent indicator for cyclic AMP in living cells. *Nat. Cell Biol.* **2**, 25-29 (1999).

12. Kojima, H., *et al.* Detection and imaging of nitric oxide with novel fluorescent indicators: diaminofluoresceins. *Anal. chem.* **70**, 2446-2453 (1998).

13. Kojima, H. & Nagano, T. Fluorescent indicators for nitric oxide. *Advanced Materials* **12**, 763-765 (2000).

14. Chalfie, M. & Kain, S. *Green fluorescent protein: properties, applications, and protocols* (Willey-Liss, 1997).

15. Tsien, R.Y. The green fluorescent protein. *Annu. Rev. Biochem* **67**, 509-544 (1998).

16. Zlokarnik, G., *et al.* Quantitation of transcription and clonal selection of single living cells with β-lactamase as reporter. *Science* **279**, 84-88 (1998).

17. Mere, L., *et al.* Miniaturized FRET assays and microfluidics: key components for ultra-high-throughput screening. *Drug Discovery Today* **4**, 363-369 (1999).

Chapter 2.

Fluorescent indicators for cyclic GMP based on cyclic GMP-dependent protein kinase Iα and green fluorescent proteins

2-1. Introduction

I have succeeded to fill the vacancy for cyclic GMP (cGMP) in an array of fluorescent indicators for major second messengers, such as Ca^{2+},[1, 2] inositol 1,4,5-triphosphate,[3] diacylglycerol,[4] cAMP[5, 6] and cGMP. I describe herein genetically encoded fluorescent indicators for cGMP in single living cells.

Upon stimulating cells with various chemicals such as nitric oxide, peptide hormones and toxins, cGMP is synthesized by catalytic conversion of GTP by soluble and particulate guanylyl cyclases[7, 8]. cGMP acts as a signaling molecule via its receptor proteins including cGMP-dependent protein kinases[9-11], cyclic nucleotide-gated cation channels[12] and cGMP-binding phosphodiesterases[13, 14], and regulates various physiological processes such as relaxation of vascular smooth muscle cells, phototransduction in retinae, epithelial electrolyte transport, bone growth and neuronal activity. Imaging the dynamics of cGMP in the single living cells is of interest not only to reveal the mechanism underlying the cellular and organ functions but also to discover or screen drugs such as phosphodiesterase inhibitors[15], which control the intracellular [cGMP], from millions of candidate compounds. However, conventional radioimmunoassay of cell lysates prepared from millions of cells,

exclusively used for analysis of total cGMP levels, does not meet those cell biological and pharmaceutical requirements.

Here I describe genetically encoded fluorescent indicators for cGMP. To construct the fluorescent indicators for cGMP, two functionally independent parts were chosen: one part is for selective molecular recognition for cGMP and the other for transducing the molecular recognition event to the generation or change in fluorescence signals. As a receptor for cGMP, cGMP-dependent protein kinase Iα (PKG Iα) was chosen based on a previous small angle X-ray scattering study by which cGMP-induced conformational change in PKG Iα has been revealed[16]. As a transducer to detect the cGMP-dependent conformational change in PKG Iα, blue- and red-shifted mutants of green fluorescent proteins (GFPs), cyan fluorescent protein (ECFP) and yellow fluorescent protein (EYFP), were fused to N- and C-terminal ends of PKG Iα, respectively. ECFP and EYFP serve as the donor and acceptor fluorophores for fluorescence resonance energy transfer (FRET), of which intensity is a function of the proximity (R) and relative angular orientation (κ) between the fluorophores[2]. cGMP is expected to alter these R and/or κ values upon its binding to PKG Iα located between the two fluorophores. The change in these FRET parameters is expected to cause cGMP-dependent changes in the observed fluorescence spectra, providing a selective and sensitive measure for intracellular concentration of cGMP, [cGMP]. The FRET between two different color GFPs has been demonstrated to be powerful to monitor Ca^{2+},[2, 17] cyclic AMP,[6] and protease activity[18, 19] in the cell. It also offers the potential for improving FRET-based fluorescent indicators replacing synthetic fluorophores such as fluorescein and rhodamine[20] with these color GFPs.

2-2. Experimental Section

2-2-1. Plasmid construction.

For constructing cDNA of CGY-FL, -A12 and -Del1-4, fragment cDNAs of $ECFP_{1-232}$, $ECFP_{1-232}$ with a C-terminal linker sequence (MDELKY), PKG Iα, PKG $_{IαL,I,C1-47A}$, PKG $Iα_{Δ1-47}$, EYFP and EYFP with an N-terminal linker sequence (YPYDVPDYAN) were generated by standard polymerase chain reaction to attach a Kozak sequence and restriction site shown in Figure 2-1. Each entire cDNA encoding CGY-FL, -A12, and -Del1-4 was subcloned at *Hind* III and *Xho* I sites of mammalian expression vector pcDNA3.1 (+) (Invitrogen Co., Carlsbad, CA).

2-2-2. Cell culture and transfection.

CHO-K1 and HEK293 cells were cultured in Ham's F-12 medium supplemented with 10 % fetal calf serum (FCS) and in Dulbecco's modified Eagle medium supplemented with 10 % FCS, 1 mM sodium pyruvate, and 0.1 mM non-essential amino acids, respectively, at 37 °C in 5 % CO_2. Cells were transfected with LipofectAMINE 2000 reagent (Life Technologies, Rockville, MD) in 24-well plates. During 12 to 24 hours after the transfection, the cells were spread onto glass bottom dishes for imaging.

2-2-3. Imaging of cells.

Before imaging, the culture medium was replaced with Hank's balanced salt solution. During 3 to 5 days after the transfection, the cells were imaged at room temperature on a Carl Zeiss Axiovert 135 microscope with a cooled CCD camera MicroMAX (Roper Scientific Inc, Tucson, AZ), controlled by MetaFluor (Universal Imaging, West Chester, PA). The exposure time at 440 ± 10 nm excitation was 50 ms. The fluorescence images were obtained through 480 ± 15 nm and 535 ± 12.5 nm filters with a 40x oil immersion objective (Carl Zeiss, Jena, Germany). To minimize an

unavoidable increase in cGMP buffering as a result of overexpression of the cGMP indicators, cells expressing high concentration of the cGMP indicators were not used for imaging as is the case of Ca^{2+} imaging reported previously.[17]

2-3. Results and Discussion

2-3-1. Design and expression of cGMP indicators, CGYs.

Mammalian PKG Iα is composed of two identical monomers. Each monomer in the dimeric kinase contains four types of functional domains as shown in Figure 2-1. The N-terminal dimerization domain is composed of a leucine/isoleucine zipper motif[21, 22]. In the absence of cGMP, PKG Iα displays a kinase inactive "closed" conformation, in which its catalytic center is occupied by an autoinhibitory domain. Upon binding of two cGMPs to the cGMP binding domains, a marked conformational change is induced, by which the autoinhibitory domain is removed from the catalytic center and PKG Iα is converted into a kinase active "open" form in its conformation[16, 23]. However, because the overall structure of PKG Iα has not been solved by X-ray diffraction or NMR, R and κ values in the tandem fusion protein of ECFP, PKG Iα and EYFP, termed CGY, are unpredictable both in the absence and presence of cGMP. I have designed three constructs, CGY-FL, -A12 and -Del1, as fluorescent indicators for cGMP as shown in Figure 2-1. CGY-FL contains a full-length PKG Iα. In contrast, the leucine/isoleucine zipper motifs of the dimerization domains in CGY-A12 and in CGY-Del1 are mutated (L,I,C1-47A) and deleted (Δ1-47), respectively, in order to avoid *inter*molecular FRET, which might possibly occur by dimerization of the indicators and complicate the fluorescence signal changes based on *intra*molecular FRET modulated by cGMP.

Chinese hamster ovary (CHO-K1) cells were transfected by a standard lipofection method with cDNAs encoding respectively CGY-FL, -A12 and -Del1 inserted in mammalian expression vectors. Figure 2-2a shows fluorescence images of the transfected cells taken by using emission filters for ECFP (480 ± 15 nm) and EYFP (535 ± 12.5 nm), showing unexpected accumulation of CGY-A12 in the nucleus. CGY-FL and CGY-Del1 were excluded from the nucleus; however, in about 30 % of

CHO-K1 cells expressing CGY-Del1, fluorescence from CGY-Del1 was observed also in the nucleus (data not shown). The leucine/isoleucine zipper motif in PKG Iα may have a role to direct its localization in the extranuclear compartment.

2-3-2. Intramolecular FRET is sensitive to cGMP-induced conformational changes in CGYs.

To evaluate the responses of the indicators for cGMP, CHO-K1 cells expressing the indicators were stimulated with 8-Br-cGMP, which is widely used as a membrane permeable and phosphodiesterase-resistant analogue of cGMP. Figure 2-2b shows pseudocolor images of ratios of 480 ±15 nm to 535 ± 12.5 nm emissions before (time 0 s) and at different time points after the addition of 1 mM 8-Br-cGMP. Figure 2-2c shows time courses of the emission ratio changes for the indicators in the cytosol. No detectable change in the emission ratio was observed for CGY-FL (Figure 2-2b, c). Also, fluorescecne intensities for ECFP and EYFP were not affected by stimulating with 8-Br-cGMP (data not shown). In contrast, a dose of 8-Br-cGMP produced a significant decrease in the emission ratio for CGY-Del1-expressing cell (Figure 2-2b, c), in which reciprocal changes in ECFP and EYFP fluorescence intensities in the cytosol were observed as shown in Figure 2-2d. These results indicate that FRET between ECFP and EYFP increases upon binding of 8-Br-cGMP to CGY-Del1. In the case of CGY-A12, 8-Br-cGMP caused a change in the emission ratio as shown in Figure 2-2b and 2c; however, the maximal change in this ratio was about one-third that for CGY-Del1.

Intramolecular FRET between GFPs in their double fusion protein is sensitive to both R and κ values due to their more rigidly fixed chromophores[2, 17, 24] than using conventional organic fluorophores[5, 20], suggesting that by inserting small linker sequences between the GFP mutants and PKG $I\alpha_{\Delta 1\text{-}47}$, the change in the emission ratio for CGY-Del1 may be improved. Several constructs containing linker

sequences between PKG $I\alpha_{\Delta 1\text{-}47}$ and GFPs were tested, three of which are schematically shown in Figure 2-1 as CGY-Del2, -Del3 and -Del4. The initial emission ratios and the emission ratio changes of CGY-Del2, -Del3 and -Del4 for 8-Br-cGMP are shown and compared with those of CGY-FL -A12 and -Del1 in Figure 2-2e. In CHO-K1 cells, CGY-Del2, -Del3 and -Del4 responded to 8-Br-cGMP; however, the linker sequences, MDELKY to the N-terminus of PKG $I\alpha_{\Delta 1\text{-}47}$ and/or YPYDVPDYAN to the C-terminus PKG $I\alpha_{\Delta 1\text{-}47}$, gave smaller effects by 8-Br-cGMP than expected on both the initial emission ratios and the changes in the emission ratio. In view of the high initial emission ratios for CGY-FL, -A12 and -Del1-4, ECFP and EYFP seem not to be closely located in the absence of cGMP due to the large size of PKG Iα, which decreases the sensitivity of FRET efficiency for the initial difference in the R value caused by the small linker insertion. Substantial deletion of PKG Iα may improve the emission ratio change of the indicator, though the responses of CGY-Del1-4 are already enough for the cGMP imaging.

Figure 2-2f illustrates the responses of CGY-Del1 for 8-Br-cGMP and 8-Br-cAMP in CHO-K1 cells, which were in concentration dependent manners for both cyclic nucleotide analogues. Approximate concentrations of the cyclic nucleotide analogues that give half maximum responses were 10^{-6} M and 10^{-4} M for 8-Br-cGMP and 8-Br-cAMP, respectively. The cyclic nucleotide selectivity of the CGY-Del1 response thus obtained is similar to that of native and wild type PKG Iα activation reported previously[25]. By using a baculovirus-mediated large-scale expression system, in vitro studies to evaluate the exact binding constants of CGYs for cGMP and cAMP may be possible.[25] From these results, I conclude that FRET from ECFP to EYFP in CGY-Dels can be a selective measure for the cellular concentration of cGMP, and the physiological concentration of cAMP does not interfere with this cGMP detection.

2-3-3. Imaging of nitric oxide-stimulated production of cGMP.

I next examined whether the indicators thus developed respond to intracellular cGMP generated upon stimulating the living cells with nitric oxide (NO). Human embryonic kidney (HEK) 293 cells[26] were transfected with cDNA of CGY-Del1. To activate the soluble guanylyl cyclase in the cell, NOC-7[27], an NO-releasing compound, was added to give its final extracellular concentration of 500 μM. NOC-7 releases NO spontaneously in a rate controlled manner. Figure 2-3a shows time courses of the NOC-7-induced changes in the emission ratio for CGY-Del1 in HEK293 cells. A significant and fast decrease in the emission ratio was followed by a slower increase in the ratio. The latter increase in the emission ratio disappeared by pretreating the cells with 100 μM zaprinast[28], a selective inhibitor for cGMP-specific phosphodiesterase, although the initial fast decrease in the emission ratio was not affected. Pretreatment of the cells with 10 μM ODQ[29], a selective inhibitor for NO-sensitive guanylyl cyclase, completely suppressed the change in the emission ratio elicited earlier by stimulating with the NO donor. Similar results were obtained by using CGY-Del2-4 (data not shown). These results indicate that CGY-Dels sufficiently work as the fluorescent indicators for [cGMP] in the single living cells.

Can the fluorescent indicators CGY-Dels then reversibly detect the fluctuation of intracellular [cGMP]? As shown in Figure 2-3b and 3c, an administration of 500 μM NOC-7 to the CGY-Del1-expressing HEK293 cell caused a rapid decrease in the emission ratio, and the subsequent recovery of the ratio to the initial level was observed. The later increase in the emission ratio is due to the degradation of cGMP by cGMP-specific phosphodiesterase as was pharmacologically examined using zaprinast in Figure 2-3a. Upon a subsequent dose of 1 mM 8-Br-cGMP, a phosphodiesterase-resistant analogue of cGMP, the recovered emission ratio was decreased again (Figure 2-3b, c). By using zaprinast instead of 8-Br-cGMP, a similar re-decrease in the recovered emission ratio was observed (Figure 2-3c). These

results demonstrate the reversible response of CGY-Del1 to fluctuating concentration of cGMP in the single living cells.

Figure 2-3d shows the response of CGY-Del1 for different concentrations of NO, 0.01 μM to 100 μM NOC-7, in HEK293 cells. At higher concentrations of NO, 10 μM and 100 μM NOC-7, cytosolic concentration of cGMP similarly increased transiently and decreased nearly to the initial level. However, at lower concentrations of NO, 1 μM and 0.1 μM NOC-7, the responses of CGY-Del1 were quite different from those at higher concentrations of NO. At 1 μM NOC-7, the rate of cGMP accumulation was faster than that at higher concentration of NOC-7, and the recovery rate of the emission ratio was slower, resulting in more prolonged duration of cGMP accumulation. At 0.1 μM NOC-7, the change in cytosolic concentration of cGMP was found not monotonous but was rather oscillation. Intracellular regulation of the activities of guanylyl cyclase and cGMP-phosphodiesterase should be responsible for the complex changes in [cGMP] observed in Figure 2-3d. For example, rapid desensitization of soluble guanylyl cyclase at higher concentration of NO[30] and allosteric or PKG-mediated phosphorylation-dependent regulation of cGMP-phosphodiesterase[15] were recently discussed. The present indicators for cGMP are thus expected to be used for discovering and understanding the cellular dynamics of cGMP, such as the cGMP oscillation, and for dissecting cGMP signaling pathways by combined use with general molecular biological techniques.

2-4. Conclusion

Fluorescence imaging is one of the most powerful techniques available for observation of the intracellular dynamics involving second messengers, exemplified by fluorescent indicators for Ca^{2+}[1, 2], cAMP[5, 6] and inositol 1,4,5-triphosphate[3]. However, fluorescent indicators for cGMP, one of the pivotal second messengers, have been left undeveloped. The analysis of cGMP has therefore exclusively depended upon conventional radioimmunoassay of cell lysates prepared from millions of cells, causing it difficult to probe the spatial and temporal dynamics of cGMP in the living cells. To overcome this limitation, I developed fluorescent indicators for cGMP. Tandem fusion proteins of ECFP, PKG $I\alpha_{\Delta 1\text{-}47}$ and EYFP were demonstrated to work as fluorescent indicators for cGMP, in which FRET was reversibly increased and decreased upon binding and dissociation of cGMP, respectively (Figure 2-4).

The cGMP indicators presented in this paper are genetically encoded, allowing further improvement of the indicators by standard mutagenesis techniques. The intracellular location of the indicator should easily be controlled by fusing with signal sequences or with proteins of interest such as guanylyl cyclases[7, 8], cyclic nucleotide-gated cation channels[12] or anchoring proteins of PKG Iα[31]. Based on previous mutagenesis studies regarding the binding domains for cyclic nucleotides[25, 32], cGMP/cAMP selectivity of the indicator may be changed, suggesting a possibility for the development of cAMP indicators consisting of single polypeptides, not the complex of GFPs-fused catalytic and regulatory domains of cyclic AMP-dependent protein kinase as was previously reported[6]. Kinase deficient mutants of the CGY-Dels may be more physiological, though no toxic effects were observed on proliferation rates of cells expressing the CGY-Dels. The present indicators for cGMP is expected to contribute to cell-based high-throughput screening[33, 34] of

potent and isoform-specific inhibitors for phosphodiesterases. Also, transgenic animals expressing the indicator for cGMP may enable non-destructive and continuous monitoring of [cGMP] levels in tissues and organs of interest before and after the administration of pharmaceuticals.

References

1. Grynkiewicz, G., Poenie, M. & Tsien, R.Y. A new generation of Ca^{2+} indicators with greatly improved fluorescence properties. *J. Biol. Chem.* **260**, 3440-3450 (1985).
2. Miyawaki, A., *et al.* Fluorescent indicators for Ca^{2+} based on green fluorescent proteins and calmodulin. *Nature* **388**, 882-887 (1997).
3. Hirose, K., Kadowaki, S., Tanabe, M., Takeshima, H. & Iino, M. Spatiotemporal dynamics of inositol 1,4,5-triphosphoate that underlies complex Ca^{2+} mobilization patterns. *Science* **248**, 1527-1530 (1999).
4. Oancea, E., Teruel, M.N., Quest, A.F.G. & Meyer, T. Green fluorescent protein (GFP)-tagged cysteine-rich domains from protein kinase C as fluorescent indicators for diacylglycerol signaling in living cells. *J. Cell Biol.* **140**, 485-498 (1998).
5. Adams, S.R., Harootunian, A.T., Buechler, Y.J., Taylor, S.S. & Tsien, R.Y. Fluorescence ratio imaging of cyclic AMP in single cells. *Nature* **349**, 694-697 (1991).
6. Zaccolo, M., *et al.* A genetically encoded, fluorescent indicator for cyclic AMP in living cells. *Nat. Cell Biol.* **2**, 25-29 (1999).
7. Nakane, M. & Murad, F. Cloning of guanylyl cyclase isoforms. *Adv. Pharmacol.* **26**, 7-17 (1994).
8. Murad, F. Regulation of cytosolic guanylyl cyclase by nitric oxide: the NO-cyclic GMP signal transduction system. *Adv. Pharmacol.* **26**, 19-33 (1994).
9. Francis, S.H. & Corbin, J.D. Progress in understanding the mechanism and function of cyclic GMP-dependent protein kinase. *Adv. Pharmacol.* **26**, 115-170 (1994).

10. Pfeifer, A., *et al.* Structure and function of cGMP-dependent protein kinases. *Rev. Physiol. Biochem. Pharmacol.* **135,** 105-149 (1999).

11. Ruth, P. Cyclic GMP-dependent protein kinases: understanding in vivo functions by gene targeting. *Pharmacol. Ther.* **82,** 355-372 (1999).

12. Zagotta, W.N. & Siegelbaum, S.A. Structure and function of cyclic nucloetide-gated channels. *Annu. Rev. Neurosci.* **19,** 235-263 (1996).

13. Sonnenburg, W.K. & Beavo, J.A. Cyclic GMP and regulation of cyclic nucleotide hydrolysis. *Adv. Pharmacol.* **26,** 87-113 (1994).

14. Juilfs, D.M., Soderling, S., Burns, F. & Beavo, J.A. Cyclic GMP as substrate and regulator of cyclic nucleotide phosphodiesterases (PDEs). *Rev. Physiol Biochem. Pharmacol.* **135,** 67-104 (1999).

15. Corbin, J.D. & Francis, S.H. Cyclic GMP phosphodiesterase-5: target of sildenafil. *J. Biol. Chem.* **274,** 13729-13732 (1999).

16. Zhao, J., *et al.* Progressive cyclic nucleotide-induced conformational changes in the cGMP-dependent protein kinase studied by small angle X-ray scattering in solution. *J. Biol. Chem.* **272,** 31929-31936 (1997).

17. Miyawaki, A., Griesbeck, O., Heim, R. & Tsien, R.Y. Dynamic and quantitative Ca^{2+} measurements using improved cameleons. *Proc. Natl. Acad. Sci. USA* **96,** 2135-2140 (1999).

18. Heim, R. & Tsien, R.Y. Engineering green fluorescent protein for improved brightness, longer wavelengths and fluorescence resonance energy transfer. *Curr. Biol* **6,** 178-182 (1996).

19. Vanderklish, P.W., *et al.* Marking synaptic activity in dendritic spines with a calpain substrate exhibiting fluorescence resonance energy transfer. *Proc. Natl. Acad. Sci. USA* **97,** 2253-2258 (2000).

20. Sato, M., Ozawa, T., Yoshida, T. & Umezawa, Y. A fluorescent indicator for tyrosine phosphorylation-based insulin signaling pathways. *Anal. Chem.* **71**, 3948-3954 (1999).

21. Ruth, P., *et al.* Identification of the amino acid sequences responsible for high affinity activation of cGMP kianse Iα. *J. Biol. Chem.* **272**, 10522-10528 (1997).

22. Atkinson, R.A., Saudek, V., Huggins, J.P. & Pelton, J.T. 1H NMR and circular dichroism studies of the N-terminal domain of cyclic GMP dependent protein kinase: a leucine/isoleucine zipper. *Biochemistry* **30**, 9387-9395 (1991).

23. Chu, D.M., Corbin, J.D., Grimes, K.A. & Francis, S.H. Activation by cyclic GMP binding causes and apparent conformational change in cGMP-dependent protein kinase. *J. Biol. Chem.* **272**, 31922-31928 (1997).

24. Nagai, Y., *et al.* A fluorescent indicator for visualizing cAMP-induced phosphorylation in vivo. *Nat. Biotechnol.* **18**, 313-316 (2000).

25. Reed, R.B., *et al.* Structural order of the slow and fast intrasubunit cGMP-binding sites of type I alpha cGMP-dependent protein kinase. *Adv. Second Messenger Phosphoprotein Res.* **31**, 205-217 (1997).

26. Bischof, G., Serwold, T.F. & Machen, T.E. Does nitric oxide regulate capasitative Ca influx in HEK 293 cells? *Cell Calcium* **21**, 135-142 (1997).

27. Hrabie, J.A., Klose, J.R., Wink, D.A. & Keefer, L.K. New nitric oxide-releasing zwitterions derived from polyamines. *J. Org. Chem.* **58**, 1472-1476 (1993).

28. Gillespie, P.G. & Beavo, J.A. Inhibition and stimulation of photoreceptor phosphodiesterase by dipyridamole and M&B 22,948. *Mol. Pharmacol.* **36**, 773-781 (1989).

29. Garthwaite, J. Potent and selective inhibition of nitric oxide-sensitive guanylyl cyclase by 1H-[1,2,4]Oxadiazolo[4,3-a]quinoxalin-1-one. *Mol. Pharmacol.* **48**, 184-188 (1995).

30. Bellamy, T.C., Wood, J., Goodwin, D.A. & Garthwaite, J. Rapid desensitization of the nitric oxide receptor, soluble guanylyl cyclase, underlies diversity of cellular cGMP responses. *Proc. Natl. Acad. Sci. USA* **97**, 2928-2933 (2000).

31. Yuasa, K., Omori, K. & Yanaka, N. Binding and phosphorylation of a novel male germ cell-specific cGMP-dependent protein kinase-anchoring protein by cGMP-dependent protein kinase Iα. *J. Biol. Chem.* **275**, 4897-4905 (2000).

32. Reed, R.B., *et al.* Fast and slow cyclic nucleotide-dissociation sites in cAMP-dependent protein kinase are transposed in type Iβ cGMP- dependent protein kinase. *J. Biol. Chem.* **271**, 17570-17575 (1996).

33. Zlokarnik, G., *et al.* Quantitation of transcription and clonal selection of single living cells with β-lactamase as receptor. *Science* **279**, 84-88 (1998).

34. Mere, L., *et al.* Miniaturized FRET assays and microfluidics: key components for ultra-high-throughput screening. *Drug Discovery Today* **4**, 363-369 (1999).

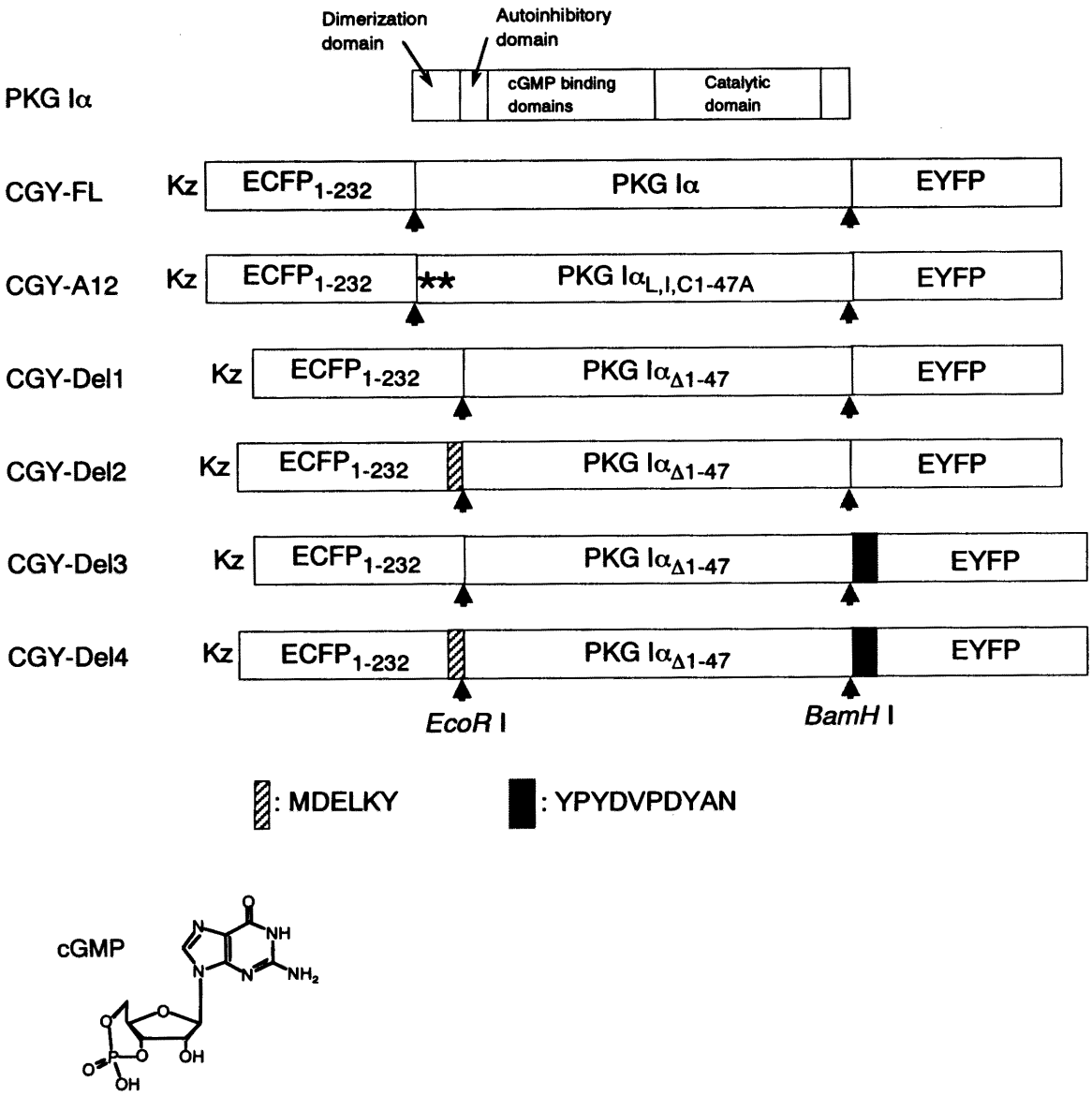

Figure 2-1. Schematic representations of domain structures of bovine cGMP-dependent protein kinase Iα (PKG Iα), CGY-FL, -A12 and -Del1-4. Two linker sequences are shown in the bottom. ECFP and EYFP are *Aequorea victoria* GFPs with mammalian codons and the following additional mutations: ECFP, F64L/S65T/Y66W/N146I/M153T/V163A/N212K, and EYFP, S65G/V68L/Q69K/S72A/T203Y. Kz is an abbreviation of a Kozak sequence, which allows optimal translation initiation in mammalian cells. Two asterisks in CGY-A12 indicate the mutation of all leucine, isoleucine and cycteine residues within 1 to 47 residues in PKG Iα to alanine.

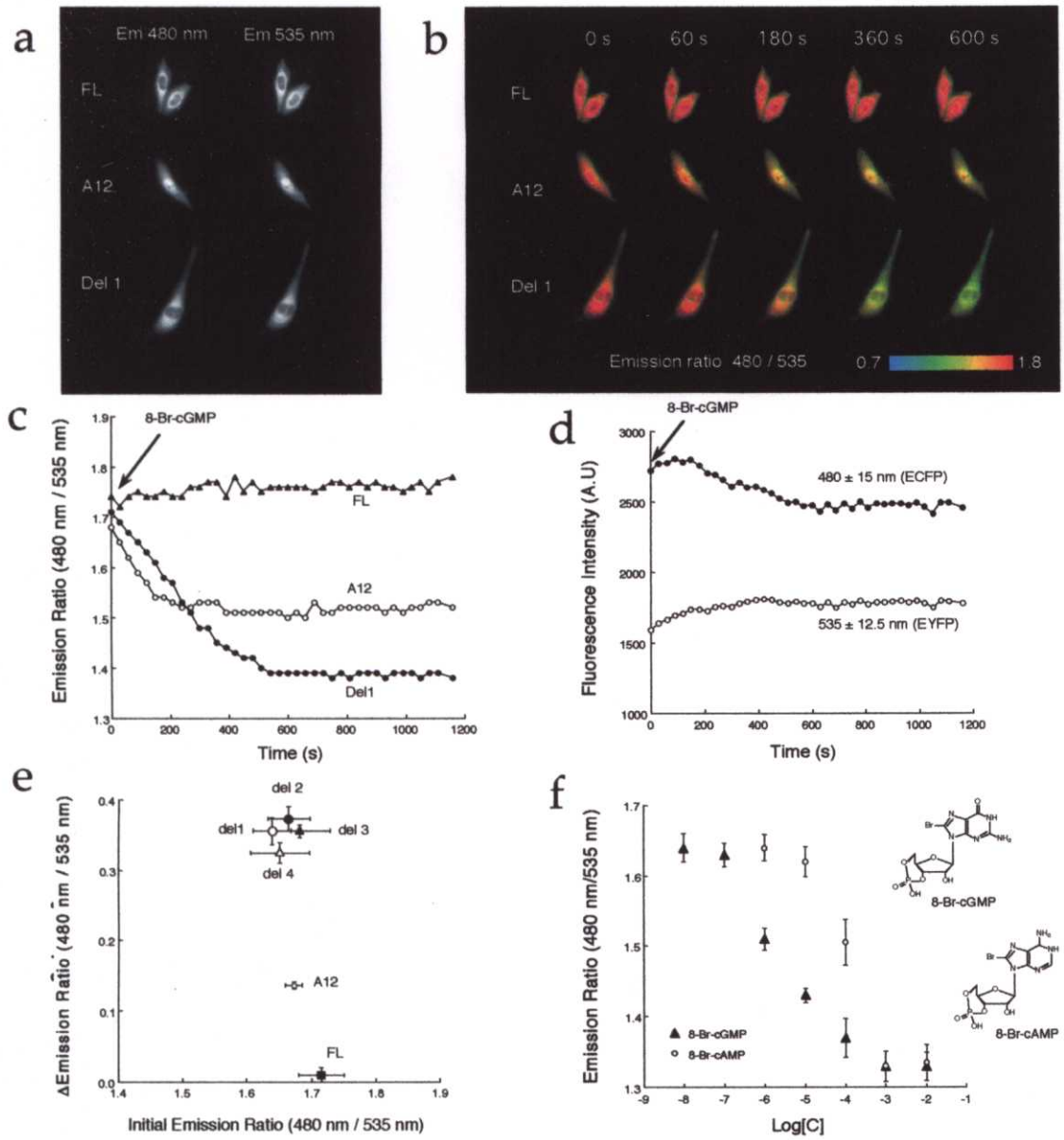

Figure 2-2. Response of CGY-FL, -A12 and -Del1-4 for 8-Br-cGMP in CHO-K1 cells. a, Fluorescence images of the cells expressing CGY-FL, -A12 and -Del1, taken using emission filters for ECFP (480 ± 15 nm) and EYFP (535 ± 12.5 nm), when excited at 440 ± 10 nm. **b,** Pseudocolor images of ratios of 480 ± 15 nm to 535 ± 12.5 nm emissions before (time 0s) and at different time intervals after the addition of 1 mM 8-Br-cGMP, obtained from the CHO-K1 cells expressing CGY-FL, -A12 and -Del1. **c,** Changes in the ratios of emissions from CGY-FL (▲), -A12 (❍) and -Del1 (●) in the cytosol, each upon stimulating with 8-Br-cGMP (Figure 2-2b). **d,** Kinetics of cytosolic fluorescence at 480 ± 15 nm (ECFP, ●) and 535 ± 12.5 nm (EYFP, ❍) from the CGY-Del1-expressing CHO-K1 cell, each upon stimulating with 8-Br-cGMP (Figure 2-2b). **e,** Comparison of the initial emission ratios and the changes in the emission ratios for CGY-FL, -A12 and -Del1-4, each upon stimulation with 8-Br-cGMP. **f,** Response of CGY-Del1 for different concentrations of 8-Br-cGMP (▲) and 8-Br-cAMP (❍) in CHO-K1 cells. CGY-Del1-expressing cells were incubated with 8-Br-cGMP or 8-Br-cAMP for 3 to 6 hours and emission ratio in the cytosol was measured on the fluorescence microscope. The results are the means and standard deviations of emission ratios from five different cells. (mean ± S.D.)

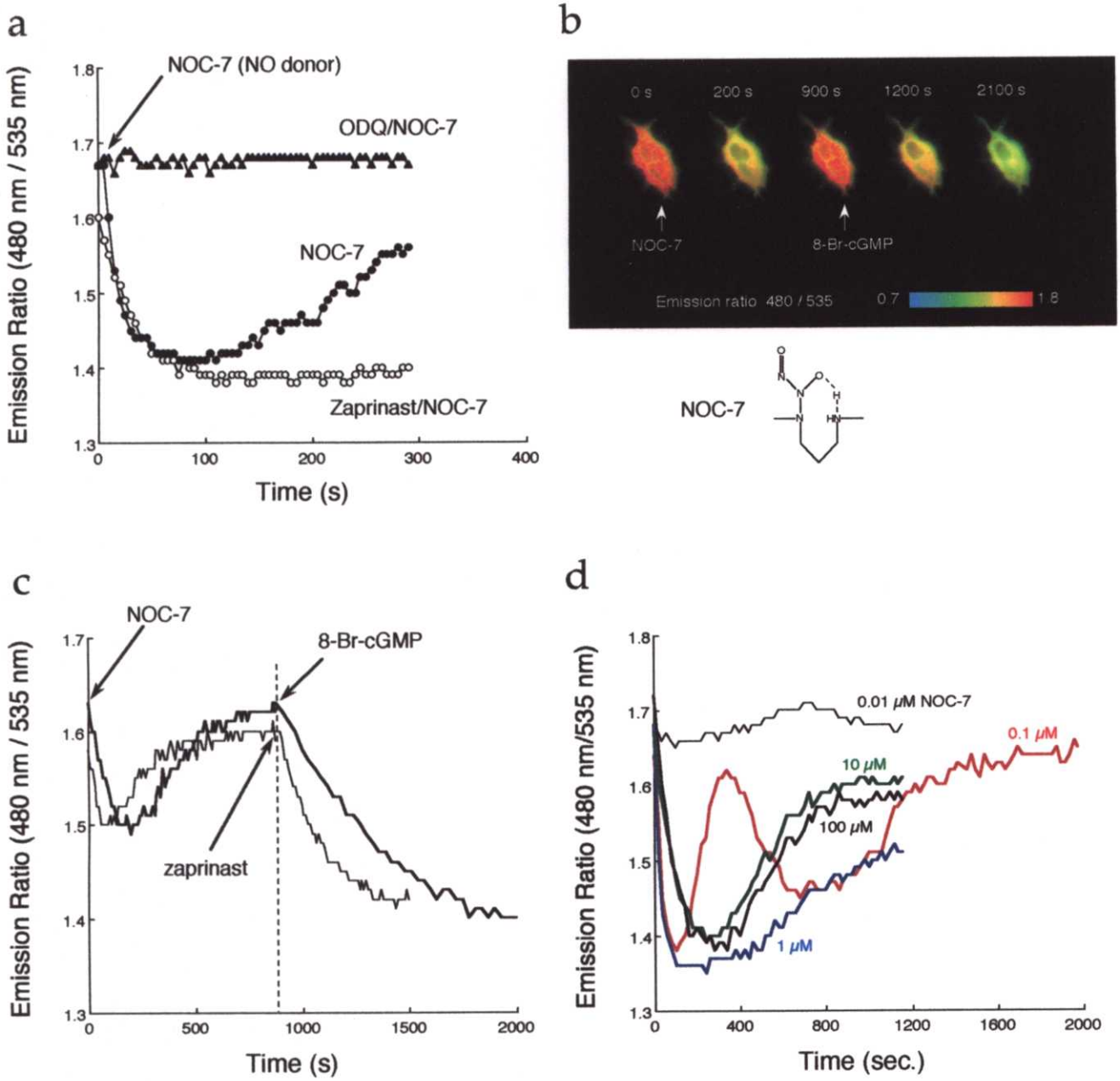

Figureu 2-3. Reversible response of CGY-Del1 for fluctuating concentration of cGMP in the living cells. **a,** Changes in the emission ratio for CGY-Del1 in the cytosol of HEK293 cells upon stimulating with 500 μ M NOC-7 (▲: the cell is pretreated with 10 μ M ODQ; ❍: the cell is pretreated with 100 μ M zaprinast.). **b,** Pseudocolor images of 480 to 535 nm emission ratios before (time 0s) and at different time points after the addition of 500 μ M NOC-7. At 900 s after addition of NOC-7, 8-Br-cGMP was added to give its final extracellular concentration of 1 mM. **c,** Changes in the emission ratios for CGY-Del1 in the cytosol of HEK293 cells upon stimulating with 500 μ M NOC-7. At 900 s after addition of NOC-7, 1 mM 8-Br-cGMP (bold line) or 100 μ M zaprinast (thin line) was added. **d,** Response of CGY-Del1 for different concentrations of NO, 0.01 μM to 100 μM NOC-7.

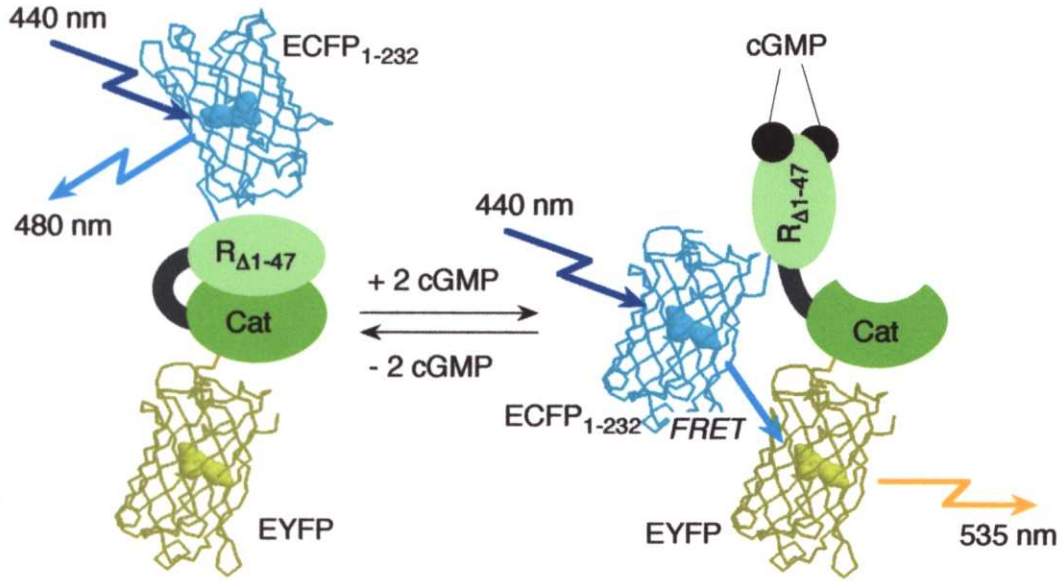

Figure 2-4. Schematic diagram showing how to detect cGMP based on FRET between ECFP and EYFP. The cylindrical β-can structure and the central chromophore of GFPs are drawn according to the crystal structure of *Aequorea victoria* GFP. The precise overall structure of PKG $I\alpha_{\Delta 1\text{-}47}$ and the relative orientations of the GFPs are not known; small angle X-ray scattering data have however revealed a marked conformational change in PKG Iα upon cGMP binding.

Chapter 3.

A Fluorescent Indicator for Tyrosine Phosphorylation-Based Insulin Signaling Pathways

3-1. Introduction

Insulin signaling pathways are initiated by binding of insulin to cell-surface insulin receptor.[1, 2] The insulin receptor is a heterotetrameric transmembrane glycoprotein, consisting of two α subunits and two β subunits linked together by disulfide bonds. Upon binding of insulin to the extracellular α subunit, insulin stimulates kinase activity of the insulin receptor and phosphorylates tyrosine residues of an intracellular substrate protein, insulin receptor substrate 1 (IRS-1). The tyrosine phosphorylation domains in IRS-1 are recognized by corresponding Src homology 2 (SH2) domain-containing enzymes such as phosphatidylinositol 3'-kinase (PI 3-kinase).[3] The tyrosine phosphorylated IRS-1 plays key roles in on/off switching of the insulin signaling pathways, serving as an interface between insulin receptor and SH2 domain-containing enzymes, which mediate insulin-induced biological responses such as glucose uptake or cell proliferation.[4]

We have reported assay methods for evaluating agonist selectivity for the insulin signaling pathways.[5, 6] Agonist-induced phosphorylation of the substrate peptide by insulin receptor was evaluated by colorimetric assay[5] or by surface plasmon resonance spectrometry[6] with the SH2 domain of PI 3-kinase. By these methods, vanadium ions and troglitazone have been found to induce insulin-like

effect without affecting kinase activity of insulin receptor and binding activity of SH2 domain of PI 3-kinase. Furthermore, it has been revealed that insulin receptor accommodated by insulin, insulin-like growth factor I (IGF-I), or insulin-like growth factor II (IGF-II) exhibited different kinase activities and the order was found to be insulin > IGF-I > IGF-II, whereas the order of Kd value has been reported to be insulin > IGF-II> IGF-I.[6]

Molecular events involved in signal transduction via protein–protein interaction as seen in the insulin signaling pathways have been analyzed almost exclusively by destructive methods such as immunoprecipitation, electrophoresis, and enzymatic assay. In contrast, fluorescent indicators for inorganic ions and small molecules such as Ca^{2+} [7-9] and cyclic AMP[10-12] have been developed, providing non-destructive methods for monitoring their spatial and temporal dynamics in single living cells. These fluorescent indicators have contributed to understand the cellular mechanism involved in signal transduction via the inorganic ions and small molecules. However, fluorescent indicators for monitoring the protein–protein interaction-based signal transduction as seen in the insulin signaling pathways remains undeveloped. The development of the fluorescent indicators not only for inorganic ions and small molecules but also for the protein–protein interaction-based signal transduction in the cell should be an active area of interest.

In this paper, a new fluorescent indicator is described for evaluating the amount of tyrosine phosphorylated substrate on the basis of insulin signaling proteins. The principle of the fluorescent indicator is schematically shown in Figure 3-1. Tetramethylrhodamine is conjugated with a synthetic phosphopeptide of 12 amino acid residues (pY939), which is derived from a tyrosine phosphorylation domain of IRS-1 and contains phosphotyrosine residue 939[13] (T-pY939). Its target, SH2N protein containing a SH2 domain of PI 3-kinase[14], is labeled with fluorescein (F-SH2N). Upon specific binding of F-SH2N with T-pY939, fluorescein (donor) and

tetramethylrhodamine (acceptor) are located within a few nanometers and fluorescence resonance energy transfer (FRET)[15-17] is induced between the fluorophores due to an overlap between donor emission and acceptor excitation spectra. FRET induced in the F-SH2N–T-pY939 complex (termed as FRET pair) results in a change in the corresponding fluorescence spectrum. Upon injection of unlabeled tyrosine phosphorylated Y939 substrate peptide, T-pY939 dissociates from F-SH2N, thereby preventing energy transfer, and resulting in the subsequent change in the fluorescence emission spectrum. This FRET pair was demonstrated to serve as a competitive fluorescent indicator for insulin-induced tyrosine phosphorylation by insulin receptor of substrate peptide Y939.

3-2. Experimental Section

3-2-1. Materials.

Escherichia coli (DH5α) cells expressing SH2N, which is a fusion protein of glutathione S-transferase and an N-terminal SH2 domain of PI 3-kinase, were kindly provided by Drs. Wataru Ogawa and Masato Kasuga (Kobe University). Chinese hamster ovary cells overexpressing human insulin receptor (CHO-HIR) were kindly provided by Dr. Takashi Kadowaki (The University of Tokyo). Chemically synthesized HPLC-purified Y939 peptide, which consists of the amino acid sequence of SEEYMNMDLGPC (expressed by one-letter abbreviations), was purchased from Biologica Co. (Nagoya, Japan). This Y939 peptide differs from its native amino acid sequence in IRS-1 by addition of a cysteine on the C-terminus of the peptide. Chemically synthesized HPLC-purified pY939 phosphopeptide, which is a synthetic tyrosine phosphorylated peptide of Y939, was purchased from Sawady Technology Co. (Tokyo, Japan). Fluorescein-5-isothiocyanate (FITC) and bicine were obtained from Dojindo Laboratories (Kumamoto, Japan). Tetramethylrhodamine-5-maleimide (TMR-MAL) was obtained from Molecular Probes Inc. (Eugene, OR). *N*-acetyl-D-glucosamine was obtained from Nacalai Tesque, Inc. (Kyoto, Japan). Other chemicals used were all of analytical reagent grade. All aqueous solutions were prepared with Milli-Q grade (>18.2 MΩ resistance) water system (Millipore Corp., Bedford, MA).

3-2-2. Apparatus.

All fluorescence measurements were performed at 25°C, using a FP-750 spectrofluorometer (JASCO Co.,Tokyo, Japan) with a quartz crystal cuvette. The pH of all solutions was measured with a glass electrode pH meter Model COM-20 (DKK Co.,Tokyo, Japan).

3-2-3. Preparation of Partially Purified Insulin Receptor.

Insulin receptor was partially purified from Chinese hamster ovary cells overexpressing human insulin receptor (CHO-HIR cells, ca. 3×10^8 cells) as described previously.[18, 19] CHO-HIR cells was scraped into 1 mL of 50 mM Tris-HCl buffer (pH 7.4) containing 2 % Triton X-100, 10 mM EDTA, 25 mM benzamidine, 2 mM BAEE, and protease inhibitors (1 mg/ml pepstatin, 1 mg/ml aprotinin, 1 mg/ml leupeptin, and 1 mM PMSF) with a cell scraper. This suspension was centrifuged (100,000 × g, 30 min, 4°C) and a clear supernatant obtained was applied to 17 mL of a wheat germ agglutinin (WGA)-Sepharose affinity column. After washing the column with 50 mM Tris-HCl buffer (pH 7.4) containing 10 mM $MgCl_2$ 0.1 % Triton X-100 and, the protease inhibitors, insulin receptor was eluted with 50 mM Tris-HCl buffer (pH 7.4) containing 300 mM *N*-acetyl-D-glucosamine and the protease inhibitors. Elution of insulin receptor was assessed by both the Bradford method[20] and binding assay with ^{125}I-insulin,[21] showing no distinguishable elution pattern (data not shown). The insulin receptor was concentrated by pressured dialysis using a Diaflo ultrafiltration membrane PM-30 (Amicon Inc., Beverly, MA) to 2 mL and stored at -80°C. The amount of total proteins was determined to be 3.2 mg by the Bradford method with γ-globulin as a standard.

The kinase activity of partially purified insulin receptor was assessed with [γ-^{32}P]ATP and random copolymers of $(Glu^{80}Tyr^{20})_n$ as a substrate for insulin receptor kinase according to the method described previously.[5, 22] The amount of the phosphorylated copolymers incubated with 2.9 μM insulin was ca. 5 times larger than that without insulin (data not shown), illustrating that the kinase-active insulin receptor was partially purified by the present method.

3-2-4. Purification of SH2N Protein.

SH2N protein was extracted and purified from *Escherichia coli* (DH5α) cells expressing SH2N as described previously.[23] The transformed *Escherichia coli* cells were cultured in LB-ampicillin medium (3.0 g polypepton, 1.5 g yeast extract, 3.0 g NaCl and 6 mg ampicillin in 300 mL Milli-Q water) at 37°C. Expression of SH2N protein was induced by addition of IPTG to give a final concentration of 0.1 mM for 8 h at 37°C. The cells were lysed in a phosphate buffer containing 1% Triton X-100 with a tip sonicator. A clear supernatant was obtained by centrifugation at 10,000 × g for 20 min at 4°C and transferred to a glutathione-affinity column. The column was washed with a phosphate buffer containing 0.1% Triton X-100. The adsorbed SH2N was eluted with a phosphate buffer (pH 8.0) containing 10 mM glutathione. The eluted SH2N was dialyzed against a phosphate buffered saline (PBS : 10 mM KH_2PO_4, 148 mM KCl, pH 7.4) for 2~3 days at 4°C. The dialyzed SH2N was stored at -80 °C. The purity of SH2N was evaluated by SDS-polyacrylamide gel electrophoresis with Coomassie Brilliant Blue staining. The purified SH2N gave a single band of 36 kDa.

3-2-5. Fluorophore labeling of SH2N protein and the peptides.

Fluorescein-labeled SH2N. The purified SH2N protein was labeled with FITC as described previously.[24] After concentration of SH2N up to 10 mg/mL by pressured ultrafiltration using a Molcut L (Nihon Millipore Ltd., Tokyo, Japan) at 4°C, the SH2N solution was adjusted to pH 8.0 with a 400 nM bicine buffer (pH8.5). Twenty μL of a FITC solution (35 mM in DMSO) was added to 500 μL of the SH2N solution with gentle stirring. The mixture was applied on a Sephadex G-25 column and eluted with PBS at 4°C. Elution of the FITC-labeled SH2N (F-SH2N) was assessed by the Bradford method and absorptiometry at 494 nm. The F-SH2N eluted was dialyzed against PBS for 2~3 days at 4°C and stored at -30°C.

Tetramethylrhodamine-labeled pY939 and Y939. Both pY939 and Y939 were labeled with TMR-MAL via its maleimide group and the C-terminal thiol group of the

peptides as described previously.[25] Five hundreds μg of the lyophilized peptide was dissolved in 100 μL of PBS. Forty μL of a TMR-MAL solution (20 mM in DMSO) was added to the peptide solution and incubated overnight at 25°C. The labeled peptides were purified by reverse phase HPLC performed on a 801-SC system (JASCO Co., Tokyo, Japan), equipped with a Kaseisorb LC ODS-300-5 column (4.6 i.d. × 250 mm long, JASCO Co., Tokyo, Japan) and a UV detector (UV-970, JASCO Co., Tokyo, Japan) under a linear gradient of 15 to 30 % acetonitrile containing 0.05 % trifluoroacetic acid at a constant flow rate of 1.0 mL/min over 45 min. Elution of the labeled peptide and the excess TMR-MAL were monitored by absorbance at 550 nm. The purified labeled peptides (T-pY939 and T-Y939) were lyophilized, dissolved into 1 mL of PBS and stored at -30°C.

3-2-6. Fluorescence Resonance Energy Transfer Assay.

Formation of the F-SH2N–T-pY939 complex (FRET pair) was evaluated as follows: Mixture solutions of F-SH2N and labeled peptides of both T-Y939 and T-pY939 in PBS were prepared in microtubes at 4°C. Concentrations of both F-SH2N and the labeled peptides were kept constant at 500 nM. The mixing ratios of T-pY939 to T-Y939 were varied as 0 : 500, 250 : 250, and 500 : 0.

Response of the FRET pair for pY939 phosphopeptide was evaluated as follows: Mixture solutions containing FRET pair and synthetic peptides of both Y939 and pY939 in PBS were prepared in microtubes at 4°C. 500 nM FRET pair and 500 nM peptides were kept constant. The mixing ratios of pY939 to Y939 were varied from 0 : 500 to 500 : 0.

All the sample mixtures were kept in darkness at 4°C for 120 min. All the fluorescence measurements were performed at 25 °C after keeping the sample mixtures for 15 min at 25°C. All the samples were excited at 488 nm. Widths of both excitation and emission slits were 5 nm and scan rate was 125 nm/min.

3-2-7 Detection of Substrate Phosphorylation by Insulin Receptor.

Insulin-dependent phosphorylation of substrate peptide Y939 by partially purified insulin receptor was evaluated with the FRET pair as follows: Sample solutions were prepared in microtubes, consisting of 0.067 % Triton X-100, 72 μg of partially purified insulin receptor preparation, 50 μM ATP, 5 mM $MnCl_2$, 50 mM Tris-HCl (pH 7.4), and each concentration of insulin. The mixture was incubated for 60 min at 4°C and the kinase reaction was initiated by adding substrate peptide Y939 to give a final concentration of 3.3 μM. The sample solutions were incubated for 120 min at 37°C with a shaker, TOMY MIXER (Tomy Seiko Co., Tokyo, Japan). The reaction mixtures were cooled at 4°C and the kinase reaction was terminated by chelating Mn^{2+} with EDTA to a final concentration of 10 mM. The FRET pair was added to each ice-cold sample mixture to give a final concentration of 500 nM. In order to equilibrate the FRET pair to dissociate in competition with the phosphorylated Y939 peptide, the microtubes were incubated for 120 min at 4°C.

3-2-8. Evaluation of Fluorescence Spectral Changes.

The changes in fluorescence spectra obtained for T-pY939 (see Figure 3-2), pY939 (see Figure 3-3), and insulin (see Figure 3-4a) were evaluated by ratios of emission intensities at 520 nm to 580 nm, which were normalized against the emission ratios for a mixture of 500 nM F-SH2N and 500 nM T-Y939, for 500 nM FRET pair solution, and for the kinase solution containing 500 nM FRET pair in the absence of insulin, respectively.

3-3. Results and Discussion

3-3-1. Characteristics of F-SH2N, T-pY939, and T-Y939.

FITC : SH2N stoichiometries in F-SH2N were determined by absorbance spectrometry and varied from 0.40 to 0.63 FITCs per SH2N protein, assuming extinction coefficients of 65 × 10^3 $M^{-1}cm^{-1}$ and 26 × 10^3 $M^{-1}cm^{-1}$ for protein-bound fluorescein at 495 nm[10] and 280 nm and 37 × 10^3 $M^{-1}cm^{-1}$ for SH2N protein at 280 nm. F-SH2Ns were termed as 0.40F-SH2N and 0.63F-SH2N, respectively, in which FITC : SH2N stoichiometries were determined to be 0.40 : 1 and 0.63 : 1. Since FITC reacts with the deprotonated amine groups of SH2N protein, only the N-terminal amine group of SH2N protein is exclusively labeled at pH 8.0 due to its lower pKa value than that of side chain amine groups such as that of lysine.[24]

TMR-MAL : peptide stoichiometries were difficult to be determined from their absorption spectra due to large differences in extinction coefficients of TMR-MAL and the peptides at 280 nm. The extinction coefficient of TMR-MAL is 18 × 10^3 $M^{-1}cm^{-1}$, which is 15 times higher than the extinction coefficient of the peptides (1.2 × 10^3 $M^{-1}cm^{-1}$) at 280 nm. Thus, the stoichiometries were estimated indirectly from the amount of TMR-MAL used for conjugation and the amount of the purified TMR-MAL-labeled peptide assessed by absorbance spectrometry at 550 nm and were ca. 95 % for both T-pY939 and T-Y939, showing no remarkable difference in reactivity of pY939 and Y939 peptide. No significant difference was observed in fluorescence spectra of T-pY939 and T-Y939 (data not shown).

3-3-2. FRET pair Formation.

Formation of a F-SH2N–T-pY939 complex (termed as FRET pair) was evaluated from changes in fluorescence emission spectra (Figure 3-2a). A fluorescence emission spectrum of F-SH2N in PBS showed its emission maximum at 520 nm (A in Figure 3-

2a), indicating no significant difference in a fluorescence emission spectrum of FITC (data not shown). A fluorescence spectrum of a mixture of F-SH2N and T-Y939 in PBS showed a slight increase in emission at 520 nm and large increase at 580 nm as compared with the spectrum of F-SH2N in PBS (B in Figure 3-2a). In contrast, with increasing the concentration of phosphopeptide T-pY939, a large decrease in emission at 520 nm and a small increase at 580 nm were observed (from B to D in Figure 3-2a).

The large increase in emission at 580 nm with T-Y939 (from A to B in Figure 3-2a) is due to direct excitation of tetramethylrhodamine in T-Y939 upon excitation at 488 nm. Since small emission of tetramethylrhodamine in both T-Y939 and T-pY939 is observed at 520 nm upon excitation at 488 nm, emission at 520 nm corresponds to emission from fluorescein in F-SH2N. The T-pY939 phosphopeptide-dependent changes in fluorescence emission spectra (from B to D in Figure 3-2a) exhibit the large decrease in emission of the donor fluorophore (fluorescein) at 520 nm and the small increase in emission of the acceptor fluorophore (tetramethylrhodamine) at 580 nm. Neither inner-filter effect in the present experimental condition nor significant difference in fluorescence properties of T-Y939 and T-pY939 like the shape and/or intensity of their emission spectra were observed (data not shown). Thus, the spectral changes from B to D in Figure 3-2a are results of FRET induced between fluorescein and tetramethylrhodamine upon specific binding of F-SH2N and T-pY939 phosphopeptide. This indicates T-pY939 phosphopeptide-dependent formation of the F-SH2N–T-pY939 complex, i.e. the FRET pair.

The observed difference in fluorescence amplitude changes at 520 nm and 580 nm was consistent with that of a fluorescent indicator reported for cyclic AMP,[10] where FRET between fluorescein and tetrametylrhodamine was evaluated. The reason why the change in fluorescence amplitude at 520 nm is larger than that at 580 nm is explained to be due to that the latter includes not only energy transfer but also a spectral overlap between emission from fluorescein at 580 nm and that from

tetramethylrhodamine at 580 nm. Emission from fluorescein at 580 nm decreases when energy transfer is induced between fluorescein and tetramethylrhodamine, though the energy transfer enhances emission from tetramethylrhodamine at 580 nm. These opposite changes cause amplitude changes at 580 nm to be less sensitive to the concentration of phosphopeptide T-pY939 as compared with those at 520 nm.

Emission at 520 nm relative to that at 580 nm decreased with increasing the concentration of phosphopeptide T-pY939 (see Figure 3-2b). The emission ratio change was found to differ between FRET pair response based on 0.40F-SH2N and that on 0.62F-SH2N as shown in Figure 3-2b. This suggests that larger change in emission at 520 nm relative to that at 580 nm is obtained with SH2N labeled with smaller amount of fluorescein.

3-3-3. Response for Synthetic Phosphopeptide.

Phosphopeptide dependent response of the FRET pair was evaluated by using Y939 peptide and pY939 phosphopeptide. Y939 peptide added to 500 nM FRET pair solution did not change the fluorescence spectrum (spectra not shown). In contrast, with increasing the concentration of phosphopeptide pY939, a large and a very small increase in emission intensities at 520 nm and at 580 nm, respectively, were observed (spectra not shown). Emission at 520 nm relative to that at 580 nm increased in a pY939 phosphopeptide dependent manner (see Figure 3-3).

In contrast to the T-pY939 phosphopeptide-dependent FRET pair formation shown above, phosphopeptide pY939 added to the FRET pair solution induced a large increase in emission at 520 nm and an increase in relative emission ratio at 520 nm and 580 nm, illustrating a decrease in energy transfer between fluorescein and tetramethylrhodamine in the FRET pair in a pY939 phosphopeptide-dependent manner. This demonstrates that the FRET pair dissociates in competition with phosphopeptide pY939, thereby preventing energy transfer and resulting in the

subsequent change in the fluorescence emission spectrum. Thus, the present FRET pair serves as a competitive fluorescent indicator for pY939 phosphopeptide.

The difference in the emission ratio change was observed between FRET pair response based on 0.45F-SH2N and the one based on 0.63F-SH2N as shown in Figure 3-3. This suggests that larger change in relative emission ratio of the FRET pair response for tyrosine-phosphorylated substrate is obtained by using SH2N labeled with smaller amount of fluorescein.

The detection limit for the tyrosine phosphorylated peptide, defined as the concentration that gives the emission ratio of three times the standard deviation of the background emission ratio, was evaluated. The background emission ratio corresponds to the emission ratio of the mixture of 500 nM FRET pair and 500 nM Y939 peptide in PBS. The detection limit thus obtained for phosphopeptide pY939 was 44 nM by using 500 nM FRET pair based on 0.45F-SH2N. In contrast, the detection limit was 47 nM pY939 phosphopeptide by using 500 nM FRET pair based on 0.63F-SH2N. This shows that there is no significant difference in the detection limit for pY939 phosphopeptide between using the FRET pair based on 0.45F-SH2N and 0.63F-SH2N.

3-3-4. Detection of Substrate Phosphorylation by Insulin Receptor.

Response for substrate phosphorylation by partially purified insulin receptor was evaluated with the FRET pair and Y939 peptide as a substrate of insulin receptor. Figure 3-4a shows the dependence of emission ratio at 520 nm to 580 nm produced by the FRET pair on insulin concentration. The emission ratio increased with increasing the concentration of insulin from ca. 1.0×10^{-9} to 1.0×10^{-6} M and then it leveled off. This illustrates insulin-dependent phosphorylation by insulin receptor of substrate peptide pY939 and the subsequent dissociation of the FRET pair in competition with the tyrosine-phosphorylated Y939 peptide.

This chemical sensing with the FRET pair was performed in the protein-rich kinase solution, where the percentage of insulin receptor among the total glycoproteins was ca. 0.6 %, estimated by binding assay with ^{125}I-insulin[21] and the method of Scatchard.[26] The median effective value (ED_{50} value) for phosphorylation of Y939 substrate peptide was obtained to be 1.0×10^{-8} M. This ED_{50} value is comparable with our previous result (2.2×10^{-8} M), based on colorimetric assay with the Y939 peptide and anti-phosphotyrosine antibody labeled with horseradish peroxidase for a kinase solution containing a small amount of protein, i.e. full purified insulin receptor.[5] In view of these results, it is concluded that the present FRET pair responds to phosphorylation by insulin receptor of the substrate peptide even in a cell-like protein-rich solution.

Response of the FRET pair for synthetic phosphopeptide pY939 in the protein-rich kinase solution, which is useful for calibrating the amount of the tyrosine phosphorylated Y939 peptide by insulin receptor, was compared with that in PBS dissolving only the FRET pair, Y939 peptide and pY939 phosphopeptide. The results obtained are shown in Figure 3-4b. The emission ratio increased with increasing the concentration of phosphopeptide pY939 in the protein-rich kinase solution. The observed range of the emission ratio was however narrower than that obtained in PBS. In order to examine the effect of surfactant Triton X-100 on this narrower range of the emission ratio observed in the protein rich-kinase solution, FRET pair response for phosphopeptide pY939 was evaluated in a solution containing FRET pair, Y939 peptide, pY939 phosphopeptide, and equal concentration of Triton X-100 with the protein-rich kinase solution. As shown in Figure 3-4b, Triton X-100 decreased the range of the emission ratio to some extent, indicating that Triton X-100 used for partially purifying insulin receptor and its kinase activity in vitro,[27] caused a decrease in the FRET pair response in the protein-rich kinase solution.

3-3-5. Comparison with the Fluorescent Substrates.

Molecular events of protein phosphorylation play key roles in the intracellular signal transduction. In order to dissect the molecular mechanism in the cell, several fluorescent substrates have been reported for monitoring kinase activities of protein kinase C,[28] calmodulin-dependent protein kinase II[29] and cyclic AMP-dependent protein kinase[30]. They are commonly based on the following chemistries for monitoring the kinase activities. Particular synthetic substrates of the kinase proteins are labeled with 6-acryloyl-2-dimethylaminonaphthalene (acrylodan),[31] which is sensitive to conformational changes in peptides attached to the fluorophore. Phosphorylation of serine residues in the fluorescent substrates changes the surrounding nature of attached acrylodan, resulting in changes in its fluorescence emission spectrum.

In contrast to this fluorescent substrate method, the present FRET pair consists of phosphopeptide pY939 and its binding protein SH2N, which are labeled with tetramethylrhodamine and fluorescein, respectively. The FRET pair dissociates in competition with unlabeled phosphopeptide pY939, serving as a fluorescent indicator for monitoring the tyrosine phosphorylation-based signal transduction. Since the phosphopeptide pY939 consists of the tyrosine-phosphorylation domain of IRS-1 and the binding domain of IRS-1 to PI 3-kinase in the cell, the present FRET pair is expected to respond to tyrosine phosphorylation not only of synthetic substrate peptide Y939 but also of endogenous substrate protein IRS-1 in the living cell. Furthermore, tyrosine phosphorylation of the substrates changes the ratio of emission intensities at two wavelengths, i.e. 520 nm and 580 nm, which may cancel out intensity variations due to probe concentrations, optical path lengths, and excitation intensities, and is highly advantageous for microscopic imaging.[32, 33] The range of the uses of fluorescence techniques based on FRET has also started to expand into

areas such as activation of protein kinase C[34] and ATP hydrolysis-induced conformational changes in myosin protein[35].

3-4. Conclusion

A fluorescent indicator was developed using pY939 synthetic phosphopeptide and its binding protein (SH2N), in which pY939 and SH2N are labeled with tetramethylrodamine and fluorescein, respectively, capable of fluorescence resonance energy transfer in the pY939–SH2N complex. This fluorescent indicator, FRET pair, was revealed to respond to unlabeled phosphopeptide pY939 in a concentration dependent manner and to tyrosine phosphorylation by partially purified insulin receptor of substrate peptide Y939 in an insulin dependent manner.

Among 21 potential tyrosine phosphorylation sites within intracellular substrate protein IRS-1, 8 tyrosine residues 460, 608, 628, 895, 939, 987, 1172, and 1222 in IRS-1 have been confirmed to be phosphorylated by insulin receptor.[36] The N-terminal SH2 domain of PI 3-kinase selectively binds with the sequences containing phosphotyrosine residues 608 and 939.[36] Upon microinjection of the FRET pair in a living cell and upon subsequent stimulation of the cell with insulin, the indicator consisting of the N-terminal SH2 domain of PI 3-kinase is expected to respond to phosphorylation of these tyrosine residues 608 and 939 in IRS-1. Other SH2 domains than SH2N from PI 3-kinase may serve as selective sensory elements for respective tyrosine phosphorylation sites in IRS-1 such as 895 and 1172, which are recognized by SH2 domains in Grb2 and SH-PTP2, respectively.[2]

The results of this study suggest that the present approach may become a general method for designing fluorescent indicators not only for tyrosine phosphorylation-based signaling pathways but also for other protein–protein interaction-based signal transduction in the living cell.

References

1. Cheatham, B. & Kahn, C.R. Insulin action and the insulin signaling networks. *Endocr. Rev.* **16**, 117-142 (1995).
2. White, M.F. The insulin signaling system and the IRS proteins. *Diabetologia* **40**, S2-S17 (1997).
3. Songyang, Z., *et al.* SH2 domains recognize specific phosphopeptide sequences. *Cell* **72**, 767-778 (1993).
4. Myers, M.G.J. & White, M.F. Insulin signal transduction and the IRS protiens. *Annu. Rev. Pharmacol. Toxicol.* **36**, 615-658 (1996).
5. Ozawa, T., Sato, M., Sugawara, M. & Umezawa, Y. An assay method for evaluating chemical selectivity of agonists for insulin signaling pathways based on agonist-induced phosphorylation of a target peptide. *Anal. Chem.* **70**, 2345-2352 (1998).
6. Yoshida, T., Sato, M., Ozawa, T. & Umezawa, Y. An SPR-based screening method for agonist selectivity for insulin signaling pathways based on the binding of phosphotyrosine to its specific binding protein. *Anal. Chem.* **72**, 6-11 (2000).
7. Grynkiewicz, G., Poenie, M. & Tsien, R.Y. A new generation of Ca^{2+} indicators with greatly improved fluorescence properties. *J. Biol. Chem.* **260**, 3440-3450 (1985).
8. Miyawaki, A., *et al.* Fluorescent indicators for Ca^{2+} based on green fluorescent proteins and calmodulin. *Nature* **388**, 882-887 (1997).
9. Miyawaki, A., Griesbeck, O., Heim, R. & Tsien, R.Y. Dynamic and quantitative Ca^{2+} measurements using improved cameleons. *Proc. Natl. Acad. Sci. USA* **96**, 2135-2140 (1999).

10. Adams, S.R., Harootunian, A.T., Buechler, Y.J., Taylor, S.S. & Tsien, R.Y. Fluorescence ratio imaging of cyclic AMP in single cells. *Nature* **349**, 694-697 (1991).

11. Bacskai, B.J., *et al.* Spatially resolved dynamics of cAMP and protein kinase A subunit in *Aplysia* sensory neurons. *Science* **260**, 222-226 (1993).

12. Hempel, C.M., Vincent, P., Adams, S.R., Tsien, R.Y. & Selverston, A.I. Spatio-temporal dynamics of cyclic AMP signals in an intact neural circuit. *Nature* **384**, 166-169 (1996).

13. Shoelson, S.E., Chatterjee, S., Chaudhuri, M. & White, M.F. YMXM motifs of IRS-1 define substrate specificity of the insulin receptor kinase. *Proc. Natl. Acad. Sci. U.S.A.* **89**, 2027-2031 (1992).

14. Piccione, E., *et al.* Phosphatidylinositol 3-kinase p85 SH2 domain specificity defined by direct phosphopeptide/SH2 domain binding. *Biochemistry* **32**, 3197-3202 (1993).

15. Stryer, L. Fluorescence energy transfer as a spectroscopic ruler. *Ann. Rev. Biochem.* **47**, 819-849 (1978).

16. Tsien, R.Y., Bacskai, B.J. & Adams, S.R. FRET for studying intracellular signaling. *Trends Cell Biol.* **3**, 242-245 (1993).

17. Selvin, P.R. Fluorescence resonance energy transfer. *Methods Enzymol.* **246**, 300-334 (1995).

18. Yarden, Y. & Schlessinger, J. Self-phosphorylation of epidermal growth factor receptor: Evidence for a model of intermolecular allosteric activation. *Biochemistry* **26**, 1434-1442 (1987).

19. Gazit, A., Yaish, P., Gilon, C. & Levitzki, A. Tyrphostin I: Sybthesis and biological activity of protein tyrosine kinase inhibitors. *J. Med. Chem.* **32**, 2344-2352 (1989).

20. Bradford, M.M. A rapid and sensitive method for the quantitation of microgram quantities of protein utilizing the principle of protein-dye binding. *Anal. Biochem.* **72**, 248-254 (1976).

21. Yamaguchi, Y.F., Choi, S., Sakamoto, Y. & Itakura, K. Purification of insulin receptor with full binding activity. *J. Biol. Chem.* **258**, 5045- 5049 (1983).

22. Braun, S., Raymond, W.E. & Racker, E. Synthetic tyrosine polymers as substrates and inhibitors of tyrosine-specific protein kinases. *J. Biol. Chem.* **259**, 2051-2054 (1984).

23. Yonezawa, K., *et al.* Insulin-dependent formation of a complex containing an 85-kDa subunit of phosphatidylinositol 3-kinase and tyrosine-phosphorylated insulin receptor substrate 1. *J. Biol. Chem.* **267**, 25958-25966 (1992).

24. Little, M.J., Paquette, D.M., Harvey, M.D. & Banks, P.R. Single-label fluorescent derivatization of peptides. *Anal. Chim. Acta* **339**, 279-288 (1997).

25. Hashida, S., *et al.* More useful maleimide compoumd for the conjugation of Fab' to horseradish peroxidase through thiol groups in the hinge. *J. Appl. Biochem.* **6**, 56-63 (1984).

26. Scatchard, G. The attraction of proteins for small molecules and ions. *Ann. N. Y. Acad. Sci.* **51**, 660-672 (1949).

27. Leray, V., Hubert, P., Cremel, G. & Staedel, C. Detergents affect insulin binding, tyrosine kinase activity and oligomeric structure of partially purified insulin receptors. *Arch. Biochem. Biophys.* **294**, 22-29 (1992).

28. McIlroy, B.K., Walters, J.D. & Johnson, J.D. A continuous fluorescence assay for protein kinase C. *Anal. Biochem.* **195**, 148-152 (1991).

29. Higashi, H., *et al.* Imaging of Ca^{2+}/calmodulin-dependent protien kinase II activity in hippocampal neurones. *NeuroReport* **7**, 2695-2700 (1996).

30. Higashi, H., *et al.* Imaging of cAMP-dependent protein kinase activity in living neural cells using a novel fluorescent substrate. *FEBS Lett.* **414**, 55-60 (1997).

31. Haugland, R.P. *Handbook of Fluorescent Probes and Research Chemicals.* 155-158 (Molecular Probes, Eugene, OR, 1996).

32. Bright, G.R., Fisher, G.W., Rogowska, J. & Taylor, D.L. Fluorescence ratio imaging microscopy. *Meth. Cell Biol.* **30**, 157-192 (1989).

33. De Bernardi, M.A. & Brooker, G. Simultaneous fluorescence ratio imaging of cyclic AMP and calcium kinetics in single living cells. *Adv. Sec. Mess. Phosph. Res.* **32**, 195-213 (1998).

34. Ng, T., *et al.* Imaging protein kinase Cα activation in cells. *Science* **283**, 2085-2089 (1999).

35. Suzuki, Y., Yasunaga, T., Ohkura, R., Wakabayashi, T. & Sutoh, K. Swingof the lever arm of a myosin motor at the isomerization and phosphate-release steps. *Nature* **396**, 380-383 (1998).

36. Sun, X.J., Crimmins, D.L., Myers, M.G., Jr., Miralpeix, M. & White, M.F. Pleiotropic insulin signals are engaged by multisite phosphorylation of IRS-1. *Mol. Cell. Biol.* **13**, 7418-7428 (1993).

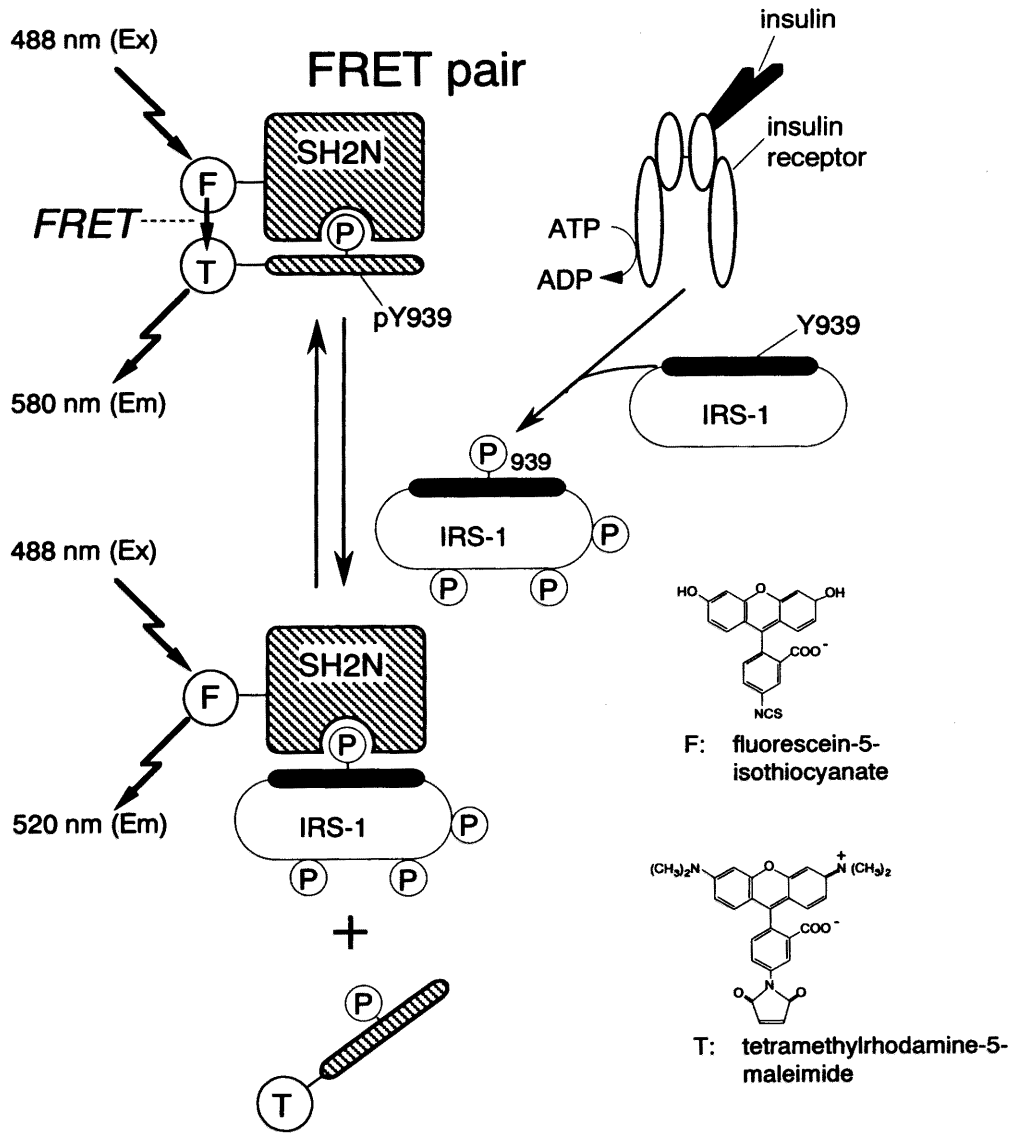

Figure 3-1. Principle of the fluorescent indicator for tyrosine phosphorylated substrates.
IRS-1 ; intracellular substrate protein that is phosphorylated by insulin-activated insulin receptor, SH2N ; fusion protein of N-terminal SH2 domain of PI 3-kinase, which is a binding unit for tyrosine phosphorylation domain of IRS-1, and glutathione S-transferase, Y939 ; synthetic peptide (SEEYMNMDLGPC) derived from tyrosine phosphorylation domain containing tyrosine residue 939 of intracellular substrate protein IRS-1, pY939 : synthetic phosphopeptide consisting of the same amino acid sequence as Y939 except for the phosphorylated tyrosine residue, F in an open circle ; fluorescein-5-isothiocyanate, T in an open circle ; tetramethylrhodamine-5-maleimide, P in an circle ; phosphotyrosine residue.
Prior to evaluation of substrate phosphorylation by insulin receptor, the fluorescein-labeled SH2N (F-SH2N) and tetramethylrhodamine-labeled pY939 (T-pY939) are mixed to form the F-SH2N–T-pY939 complex (FRET pair), where fluorescence resonance energy transfer (FRET) is induced between the two fluorophores. The FRET pair injected into a kinase reaction solution or in an insulin-stimulated living cell dissociates in competition with the tyrosine phosphorylated substrate, resulting in disappearance of this FRET mode.

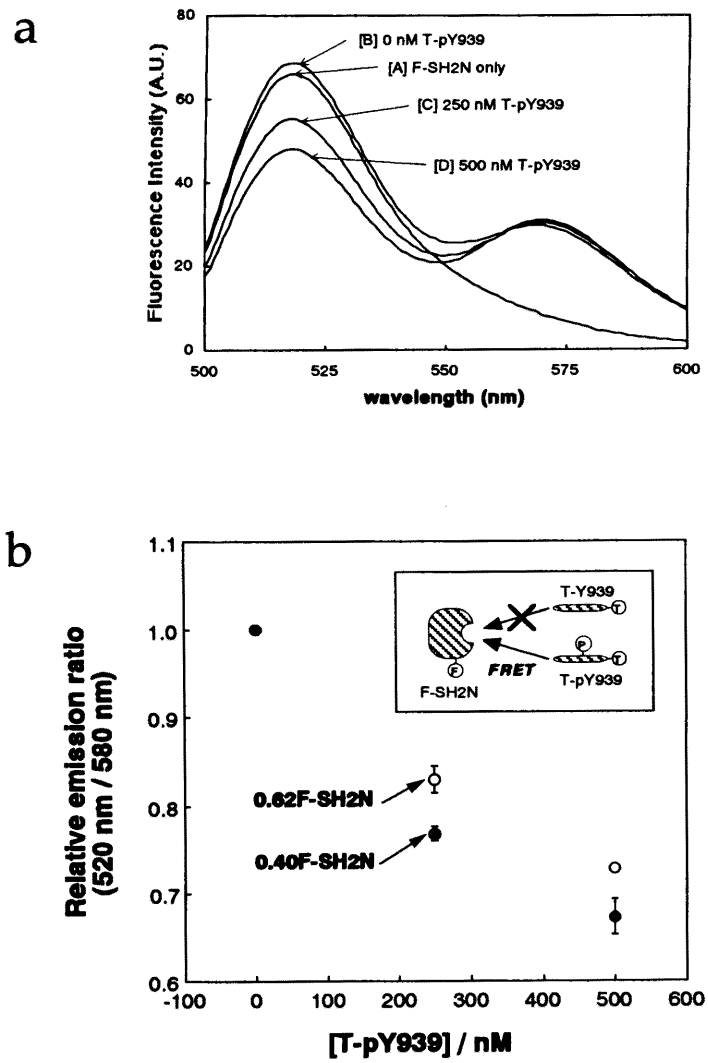

Figure 3-2. (a) Dependence of changes in fluorescence emission spectra on the concentration of T-pY939 phosphopeptide. The concentration of T-pY939 phosphopeptide among 500 nM peptides (T-Y939 peptide and T-pY939 phosphopeptide) added to the F-SH2N solution was changed from 0 to 500 nM. The compositions of each sample solution in PBS were as follows: [A] 500 nM F-SH2N, [B] 500 nM F-SH2N and 500 nM T-Y939, [C] 500 nM F-SH2N, 250 nM T-Y939 and 250 nM T-pY939, and [D] 500 nM F-SH2N and 500 nM T-pY939. (b) Dependence of relative emission ratios at 520 nm to 580 nm on the concentration of T-pY939 phosphopeptide. The horizontal axis is expressed as the concentration of T-pY939 phosphopeptide among 500 nM peptides (T-Y939 and T-pY939). FITC : SH2N stoichiometries in 0.40 F-SH2N and in 0.62F-SH2N were determined to be 0.40 : 1 and 0.62 : 1, respectively, by absorbance spectrometry. The results are the means and standard deviations of three separate experiments (mean ± S.D.).

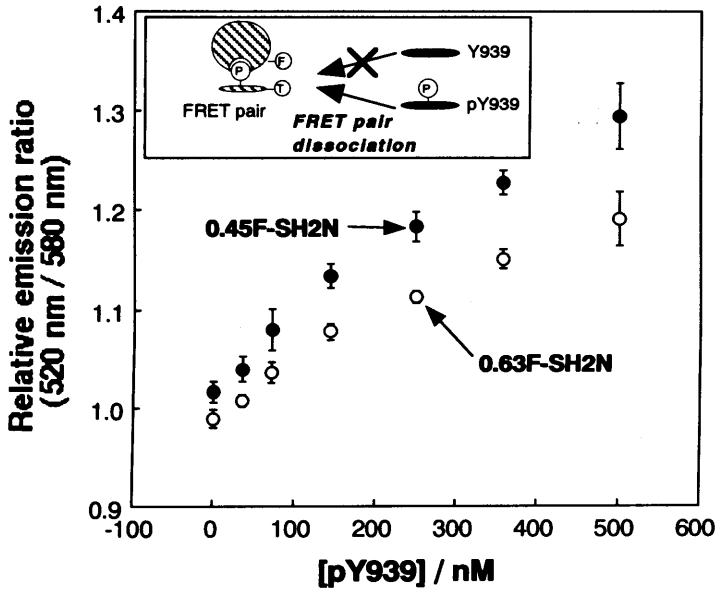

Figure 3-3. Dependence of relative emission ratios at 520 nm to 580 nm on the concentration of pY939 phosphopeptide. The horizontal axis is expressed as the concentration of pY939 phosphopeptide among 500 nM peptides (Y939 and pY939). The results are the means and standard deviations of three separate experiments (mean ± S.D.).

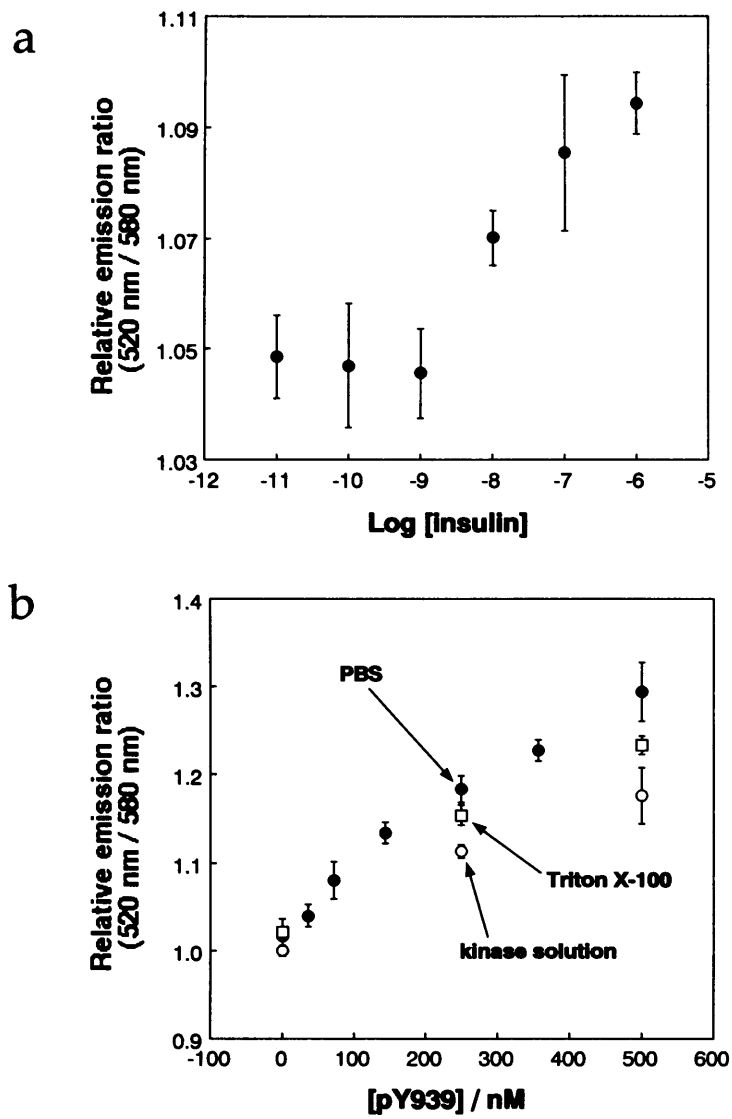

Figure 3-4. (a) Dependence of the concentration of tyrosine phosphorylated Y939 substrate peptide on the concentration of human insulin. Insulin was dissolved in 50 mM Tris-HCl buffer (pH 7.4) containing 0.067 % Triton X-100, 50 μM ATP, 5 mM $MnCl_2$, 3.3 μM Y939 substrate peptide and, 72 μg of partially purified insulin receptor preparation. The concentration of insulin ranged from 1×10^{-11} to 1×10^{-6} M. The concentration of tyrosine phosphorylated Y939 peptide was evaluated with the FRET pair added to give a final concentration of 500 nM. The results are the means and standard deviations of three separate experiments (mean ± S.D.). (b) Responses of the FRET pair for pY939 phosphopeptide in PBS (●), in the kinase solution shown in Figure 3-4a without insulin (O) and in 50 mM Tris buffer (pH 7.4) containing equal concentration of Triton X-100 with the kinase solution shown in Figure 3-4a (□). The results are the means and standard deviations of three separate experiments (mean ± S.D.).

Chapter 4.

Genetically Encoded Fluorescent Indicators for Imaging Protein Phosphorylation in Single Living Cells

4-1. Introduction

Protein phosphorylation by intracellular kinases plays one of the most pivotal roles in signaling pathways within cells[1]. The kinase proteins catalyze transfer of the γ phosphate of ATP and phosphorylation of hydroxyl groups of serines, threonines and/or tyrosines on the substrate proteins. Upon this phosphorylation, the substrate proteins are subject to conformational changes due to negative charges of the phosphates, which subsequently triggers their enzymatic activation and interaction with their respective target proteins. To reveal the biological issues related to the kinase proteins, electrophoresis, immunocytochemistry and in vitro kinase assay have been used. Recently, Bastiaens' and Parker's groups have improved an immunofluorescence staining method to detect protein phosphorylation in the cells and tissues[39]. However, these conventional methods do not provide enough information about spatial and temporal dynamics of the signal transduction based on protein phosphorylation and dephosphorylation in living cells. In contrast to the kinase signaling, second messenger signaling, such as Ca^{2+}[2-4], inositol 1,4,5-triphosphate[5], diacylglycerol[6], cyclic AMP[7, 8] and cyclic GMP[9], have been visualized using fluorescent indicators in single living cells. The measurements based on those

fluorescent indicators have been found to provide a high spatial and temporal resolution enough for dissecting the single cell events of the second messengers[10].

To overcome the limitation for investigating the kinase signaling, I describe herein genetically encoded fluorescent indicators for visualizing the protein phosphorylation in living cells. The principle of the present method is schematically shown in Figure 4-1. A substrate domain for a kinase protein of interest is fused with a phosphorylation recognition domain via a flexible linker sequence. The tandem fusion unit consisting of the substrate domain, linker sequence and phosphorylation recognition domain, is sandwiched with two different color fluorescent proteins, cyan fluorescent protein (CFP) and yellow fluorescent protein (YFP), which serve as the donor and acceptor fluorophores for fluorescence resonance energy transfer (FRET)[9, 11, 12]. As a result of phosphorylation of the substrate domain and subsequent binding of the phosphorylated substrate domain with the adjacent phosphorylation recognition domain, FRET is induced between the two fluorescent units, which causes the phosphorylation-dependent changes in fluorescence emission ratios of the donor and acceptor fluorophores. Upon activation of phosphatases, the phosphorylated substrate domain is dephosphorylated and the FRET signal is decreased. I named this indicator "phocus" (a fluorescent indicator for protein phosphorylation that can be custom-made). As the phosphorylation recognition domain within phocus, not only endogenous domains such as src homology 2 (SH2) domains[13], phosphotyrosine binding (PTB) domains[14] and WW domains[15] but also single chain antibodies (scFvs)[16, 17] immunized with the phosphorylated substrate sequences of interest are available. Thus, the present method has more general applicability for kinase signaling in the living cell compared with previously reported fluorescent indicators[18-21] based on uncontrollable conformational changes in substrate peptides themselves upon phosphorylation.

4-2. Experimental Section

4-2-1. Materials.

Human insulin was purchased from Petide Institute, Inc. (Osaka, Japan). Ham's F-12 medium, fetal calf serum, Hank's balanced salt solution and LipofectAMINE 2000 reagent were obtained from Life Technologies (Rockville, MD). Human insulin receptor and tyrphostin 25 were purchased from Sigma Chemical Co. (St. Louis, MO). Anti-phosphotyrosine antibody (PY20) and anti-β-subunit of human insulin receptor antibody were purchased from Santa Cruz Biotechnology, Inc. (Santa Cruz, CA). Anti-GFP antibody was obtained from Clontech (Palo Alto, CA). Anti-rabbit IgG antibody labeled with Cy5 was obtained from Jacson ImmunoResearch Lab,. Inc. (Pennsylvania, PA). Other chemicals used were all of analytical reagent grade.

4-2-2. Plasmid construction.

For constructing cDNAs of phocuses, fragment cDNAs of ECFP, EYFP, substrate domain, phosphorylation recognition domain and PH-PTB domain from human insulin receptor substrate-1 (IRS-$1_{1\text{-}271}$) were generated by standard polymerase chain reaction (PCR) to attach restriction site shown in Figure 4-2. All cloning enzymes were from Takara Biomedical (Tokyo, Japan) and were used according to the manufacture's instructions. All PCR fragments were sequenced with ABI310 genetic analyzer.

The amino acid sequence of the substrate domain (Y941) is ETGTEEYMKMDLG, which is a tyrosine-phosphorylation domain by insulin receptor[22] within insulin receptor substrate-1 (IRS-1). The phosphorylation recognition domain is an N-terminal SH2 domain (SH2n) from p85 subunit ($p85_{330\text{-}429}$) of bovine phosphatidylinositol 3-kinase, which is reported to bind with the phosphorylated substrate domain within the IRS-1 protein[23]. The amino acid

sequence of the nuclear-export-signal sequence (nes) is LPPLERLTL, which is derived from a human immunodeficiency virus-derived protein, Rev[40]. Each of entire cDNA encoding phocuses was subcloned at *Hind* III and *Xba* I sites of a mammalian expression vector, pcDNA3.1 (+) (Invitrogen Co., Carlsbad, CA). For bacterial expression, each cDNA encoding phocus-1 and -2 was subcloned in pRSET-A (Invitrogen Co., Carlsbad, CA).

4-2-3. Cell culture and transfection.

CHO-IR cells overexpressing human insulin receptor were cultured in Ham's F-12 medium supplemented with 10 % fetal calf serum at 37 °C in 5 % CO_2. Cells were transfected with LipofectAMINE 2000 reagent. During 12 to 24 hours after the transfection, the cells were spread onto glass bottom dishes, glass coverslips or plastic culture dishes for fluorescence imaging of living cells, immunofluorescence or western blotting analysis, respectively.

4-2-4. Immunoprecipitation and immunoblot analysis.

CHO-IR cells expressing phocus-1 and -2 were stimulated with 100 nM insulin for 20 min at 25 °C. The cells were lysed with an ice-cold lysis buffer (50 mM Tris-HCl, pH 7.4, 100 mM NaCl, 1 mM EDTA, 0.1 % Triron X-100, 10 mM NaF, 2 mM sodium orthovanadate, 1 mM PMSF, 10 μg/mL pepstatin, 10 μg/mL leupeptin, 10 μg/mL aprotinin). The phocuses were immunoprecipitated from the whole cell lysates of the CHO-IR cells with anti-GFP antibody for 2 hours at 4 °C. Protein G-Sepharose 4FF beads were used to adsorb the immunoprecipitates and then wash four times with an ice-cold washing buffer (50 mM Tris-HCl, pH 7.4, 100 mM NaCl, 1 mM EDTA, 0.1 % Triron X-100, 10 mM NaF, 2 mM sodium orthovanadate, 1 mM PMSF, 10 μg/mL pepstatin, 10 μg/mL leupeptin, 10 μg/mL aprotinin). The samples were separated by SDS-polyacrylamide gel electrophoresis, and electrophoretically transfered onto

PVDF membrane. The membrane was probed with anti-phosphotyrosine antibody (PY20, 1 : 500 dilution).

4-2-5. Imaging of cells.

After serum starvation with a serum-free medium, the culture medium was replaced with a Hank's balanced salt solution for imaging. As described previously[9], during 3 to 5 days after the transfection, the cells were imaged at room temperature on a Carl Zeiss Axiovert 135 microscope with a cooled CCD camera MicroMAX (Roper Scientific Inc, Tucson, AZ), controlled by MetaFluor (Universal Imaging, West Chester, PA). The exposure time at 440 ± 10 nm excitation was 100 ms. The fluorescence images were obtained through 480 ± 15 nm and 535 ± 12.5 nm filters with a 40x oil immersion objective (Carl Zeiss, Jena, Germany).

4-2-6. Immunofluorescence microscopy.

CHO-IR cells expressing phocus-2pp were stimulated with 100 nM insulin for 7 min at 25 °C. The cells were fixed with 2% paraformaldehyde and were permeabilized with a phosphate-buffered saline containing 0.2% Triton X-100 for 10 min. After 45 min of incubation with rabbit anti-β-subunit of human insulin receptor antibody (1 : 100 dilution), the cells were washed with a phosphate-buffered saline containing 0.2 % fish skin gelatin and incubated with anti-rabbit IgG antibody labeled with Cy5 (1 : 500) for 30 min. The coverslips were mounted onto the slide and observed with a confocal laser scanning microscope (LSM 510, Carl Zeiss).

4-3. Results and Discussion

Tyrosine kinase receptors such as insulin receptor and growth hormone receptors function at the beginning of a number of signal transduction cascades, whereas nonreceptor tyrosine kinases and serine/threonine kinases function throughout signaling cascades[1]. In the present study, development and applicability of phocus was exemplified using insulin signaling proteins for imaging protein phosphorylation by insulin receptor. Phocus contains a tandem fusion unit of a substrate domain of interest, flexible linker sequence and phosphorylation recognition domain (Figure 4-1). As the substrate domain within phocus, a tyrosine phosphorylation domain (Y941) derived from insulin receptor substrate-1 (IRS-1) is used, in which insulin receptor phosphorylates the tyrosine residue 941 in an insulin dependent manner[22]. Its target, an N-terminal SH2 domain (SH2n) of p85 regulatory subunit of phosphatidylinositol 3-kinase was chosen as the phosphorylation recognition domain[23]. Figure 4-2 shows schematic representations of phocuses tested here. The central unit sandwiched with GFPs is different between phocus-1 and -2, where the order of the SH2n and Y941 is reversed. To examine which central units of phocus-1 and -2 are efficiently phosphorylated by insulin receptor, in vitro and in vivo phosphorylation assays were performed. Phocus-2 purified from bacteria was well phosphorylated by insulin receptor in insulin and time dependent manners as shown in Figure 4-3a, whereas the phosphorylation rate of purified phocus-1 was slower than that of phocus-2 in vitro. The difference in the extent of phosphorylation was observed between phocus-1 and -2 also in vivo (Figure 4-3b). These results indicate that phocus-2 is a better substrate than phocus-1 in vitro and in vivo. In view of the X-ray crystal structure of insulin receptor in complex with a substrate peptide derived from IRS-1[24], the difference in the phophorylation efficiency between phocus-1 and -2 may be ascribed to the

difference in steric effect adjacent to C-terminus of Y941, due to YFP and flexible linker for phocus-1 and -2, respectively.

To test whether the phosphorylated phocus-2 is dephosphorylated by endogenous protein tyrosine phosphatases in living cells, CHO-IR cells expressing phocus-2 were stimulated with 100 nM insulin, washed, cultured in serum-free medium, and immunoblotting analysis with phosphotyrosine antibody was performed. As shown in Figure 4-3c, phocus-2 phosphorylated by insulin receptor was efficiently dephosphorylated in a time dependent manner in CHO-IR cells. This indicates that intramolecular interaction of the phosphorylated Y941 with the adjacent SH2n within phocus-2 does not block dephosphorylation of the phosphorylated Y941 by endogenous tyrosine phosphatases. Thus, phocus-2 can provide a reversible record of tyrosine kinase activity of insulin receptor in living cells.

I next examined whether the efficiency of FRET increases after phosphorylation of phocus-2 by insulin receptor. CHO-IR cells were transfected with the cDNA encoding phocus-2 inserted in a mammalian expression vector. Figure 4-4a shows a fluorescence image of a phocus-2-expressing cell taken by using an emission filter for CFP (480 nm ± 15 nm), which indicates that phocus-2 uniformly distributes both in the cytosolic compartment and in the nucleus. To evaluate the response of phocus-2 for its phosphorylation, CHO-IR cells expressing phocus-2 were stimulated with 100 nM insulin. Figure 4-4b shows pseudocolor images of emission ratios of 480 ± 15 nm for CFP to 535 ± 12.5 nm for YFP, when excited at 440 ± 10 nm, before and at different times after insulin stimulation. Figure 4-4c shows time courses of the emission ratio changes in the cytosol and in the nucleus. A dose of insulin caused a rapid and significant decrease in the cytosolic emission ratio for the phocus-2-expressing cells, whereas the emission ratio in the nucleus did not change significantly (Figures 4-4b and 4-4c). The insulin-induced change in emission ratio

in the cytosol was completely suppressed when the cells were pretreated with 500 μM tyrphostin 25, an inhibitor for insulin receptor, as shown in Figure 4-4d. As a negative control, CHO-IR cells expressing phocus-2A, in which there is a substitution of tyrosine to alanine at the phosphoacceptor site within the substrate domain, were stimulated with insulin, however, no significant change in the cytosolic emission ratio was observed (Figure 4-4d). Also, phocus-2R358A gave no significant response, in which SH2n was replaced by SH2nR358A[25] to inhibit its binding with the phosphorylated Y941 (Figure 4-4d). These results demonstrate that FRET from CFP to YFP is increased upon tyrosine-phosphorylation of the Y941 within phocus-2 in the cytosolic compartment and the subsequent binding of the phosphorylated Y941 with the adjacent phosphorylation recognition domain SH2n, which allows visualization of protein phosphorylation by insulin receptor in single living cells using phocus-2.

Why was no significant FRET signal observed in the nucleus of phocus-2-expressing cells? Upon insulin stimulation, emission from CFP and that from YFP showed reciprocal changes in the cytosol due to phosphorylation-dependent energy transfer, and the emissions from CFP and YFP were followed by their continuous increases as shown in Figure 4-4e. On the other hand, the both emissions continuously decreased in the nucleus during the insulin stimulation. These results show continuous translocation of phocus-2 from the nucleus to cytosol. This insulin-dependent translocation was not observed for phocus-2A-expressing cells (Figure 4-4f), which indicates that the translocation of phocus-2 is not ascribed to interaction of phocus-2 with cytosolic phosphoproteins, such as IRSs, via the SH2n within phocus-2. Thus, a rigidly packed conformation of the phosphorylated phocus-2 is thought to be responsible for no significant FRET signal in the nucleus, by which the phosphorylated phocus-2 might be segregated in the cytosolic compartment without entering into the nucleus through nuclear pores. On the other

hand, a floppy conformation of the unphosphorylated phocus-2, due to the flexible linker sequence within phocus-2, might enable its free traffic through nuclear pores.

To eliminate phocus-2 from the nucleus, where FRET was not changed upon insulin stimulation, phocus-2nes that have a nuclear-export-signal sequence, LPPLERLTL, was developed No significant fluorescence was observed from the nucleus of a phocus-2nes-expressing cell, which indicates that the fluorescent indicator, phocus-2nes, was removed as expected from the nucleus (Figure 4-5a). Upon stimulating cells expressing phocus-2nes with 100 nM insulin, a progressive decrease in the cytosolic emission ratio was observed as shown in Figure 4-5a. No significant difference was observed in the time course of the phocus-2 response and that of the phocus-2nes response. Figure 4-5b shows the response of phocus-2nes to differing concentrations of insulin in CHO-IR cells. The accumulation rate of phosphorylated phocus-2nes by insulin receptor was increased in parallel with increasing insulin concentration from 1 nM to 100 nM. At 0.1 nM insulin, no significant accumulation of the phosphorylated phocus-2nes was observed. This insulin dose-response for the emission ratio change of phocus-2nes was similar to that for tyrosine phosphorylation of native IRS-1 protein in the cell, which was previously examined by conventional autoradiography[26].

Phocus-2nes is more advantageous than phocus-2 for multi-cell analysis with a fluorescence multi-well plate reader, with which the indicator protein in the cytosol and that in the nucleus can not be discriminated. Unphosphorylated nuclear phocus-2 could be subject to the decreased change in the net emission ratio when analyzed with the multi-well plate reader, whereas phocus-2nes existing only in the extranuclear compartment is phosphorylated by insulin receptor and entirely contribute to the net emission ratio change. Taking advantage of phocus-2nes, high-throughput screening of anti-diabetic small molecules, such as L-783,281 that was

discovered to directly stimulate the kinase activity of insulin receptor[27, 28], should be possible among thousands of candidate chemicals using phocus-2nes.

Signaling proteins, such as kinases, phosphatases and their substrates, are often discretely localized in the cell and are organized to build signaling domains by extracellular stimuli[1]. This mechanism is thought to be a critical determinant for efficiency and specificity of signal transmission in the cell. IRS-1, the endogenous substrate protein for insulin receptor, contains a pleckstrin homology (PH) and a phosphotyrosine binding (PTB) domain to its N-terminal end[29]. The PH and PTB domain bind with the phosphoinositides at the membrane and with the juxtamembrane domain of insulin receptor, which is tyrosine-phosphorylated by insulin stimulation, respectively[30]. Thus, the concentration of IRS-1 is increased around insulin receptor at the plasma membrane upon insulin stimulation, which underlies efficient and selective phosphorylation of IRS-1 by insulin receptor[31, 32]. The present fluorescent indicator, phocus-2, was fused with the PH-PTB domain derived from the IRS-1 protein to construct phocus-2pp as shown in Figure 4-2. Phocus-2pp was phosphorylated upon insulin stimulation in vivo as shown in Figure 4-6a, however, insulin-dependent interaction of the phosphorylated phocus-2pp was detected neither with insulin receptor (95 kDa) nor IRS-1 (185 kDa) using the immunoprecipitation and immunoblotting with phosphotyrosine antibody. The insulin stimulation triggered a significant change in CFP/YFP emission ratio in the cytosol (Figure 4-6b). Figure 4-6c shows a comparison of the cytosolic emission ratio change for phocus-2pp and that for phocus-2 when stimulated with 100 nM insulin. The rate of the cytosolic emission ratio change for phocus-2pp was significantly faster than that for phocus-2, though the both emission ratios when they reached plateaus were not significantly different. This indicates that by introducing the endogenous targeting domain within IRS-1, the phosphorylation rate of phocus-2pp by the activated insulin receptor was enhanced, which gives a more physiological basis for

imaging the localized kinase signaling in the living cells using fluorescent indicators. Phosphorylation of phocus-2pp could be visualized also in cultured cells such as L6 cells, where insulin receptor was expressed at a lower level than that in the CHO-IR cells (data not shown).

Also, upon insulin stimulation, dot-like structures, where phocus-2pp was accumulated, appeared around the plasma membrane after phosphorylation of phocus-2pp reached a plateau, and disappeared in 1000 seconds (Figure 4-6b, 460s and 1000s, respectively). Confocal fluorescence images illustrate insulin-dependent formation of dot-like structures containing insulin receptor and colocalization of phocus-2pp with insulin receptor at the dot-like structures (Figure 4-6d). During the formation of the dot-like structures, concentration of the cytosolic phocus-2pp was decreased (Figure 4-6e, form 0 to 500 seconds), which indicates translocation of the cytosolic phocus-2pp to the dot-like structures via the PH-PTB domain within phocus-2pp. At the dot-like structures, the insulin-dependent change in CFP/YFP emission ratio was found to be larger than that at the nucleus and cytosol (Figure 4-6f). This indicates a gradient of phosphorylated phocus-2pp from the dot-like structures to cytosol, which is probably due to difference in balance of kinase and phosphatase activities there. When the dot-like structures were disappeared after insulin stimulation (Figure 4-6b, 1000s), retranslocation of phocus-2pp to the cytosol was observed (Figure 4-6e, form 500 to 1000 seconds). On the other hand, the nuclear phocus-2pp continuously translocated to the cytosol during the insulin stimulation (Figure 4-6e), as was observed for phocus-2 (Figure 4-4e). Although molecular mechanisms that explain the formation and disappearance of the dot-like structures containing insulin receptor are remained to be clarified, phocus-2pp should contribute to reveal the biological significance of the tyrosine kinase signaling in the characteristic dot-like structures, with high spatial and temporal resolution.

Compared with phocus-2pp, phocus-2 did not show any significant subcellular localization, including the plasma membrane, upon insulin stimulation (Figure 4-4b). From this result, it is suggested that upon insulin stimulation, SH2n within phocuses preferentially binds via *intra*molecular reaction with the adjacent phosphorylated Y941 rather than binding via *inter*molecular reaction with the other localized phosphoproteins such as endogenous IRS proteins[33, 34]. Although physiological effects by the expression of the indicator proteins remain to be worked out, this *intra*moleccular binding of phosphorylated Y941 and SH2n domains within phocuses may be due to normal growth of cells expressing phocuses without highly buffering tyrosine kinase signaling in the living cells.

4-4. Conclusion

In conclusion, I developed a method for visualizing the protein phosphorylation-based signal transduction in the living cells, which was herein exemplified for insulin signaling pathways. The phocuses contain one of phosphorylation domains of IRS-1. Although the IRSs are prominent substrates of insulin receptor, several other tyrosine kinases, such as insulin-like growth factor receptors and JAKs, are known to phosphorylate the IRSs[35]. The phocuses are thus expected to be used also for visualizing their kinase activities. The present method is advantageous not only for imaging the kinase signaling in single live cells with high spatial and temporal resolution, but also for multi-cell analysis aimed at high-throughput screening of pharmaceuticals[36, 37] that regulate kinase and phosphatase activities, though further improvements of the present phocuses will be necessary. Thanks to the GFP mutants and genetical techniques, I could improve my earlier approach[38] using synthetic FRET fluorophores, fluorescein and rhodamine, to the present genetically encoded indicators, with which nondestructive and continuous monitoring of protein phosphorylation-based signaling events may be possible in tissues and organs of interest in transgenic animals expressing the present phocuses. For general applicability, the endogenous phosphorylation-recognition domain within the present indicators could be replaced with single chain antibodies (scFvs)[16, 17] against the phosphorylated substrate sequences of interest, and it is now under examination.

References

1. Hunter, T. Signaling—2000 and beyond. *Cell* **100**, 113-127 (2000).
2. Grynkiewicz, G., Poenie, M. & Tsien, R.Y. A new generation of Ca^{2+} indicators with greatly improved fluorescence properties. *J. Biol. Chem.* **260**, 3440-3450 (1985).
3. Miyawaki, A., *et al.* Fluorescent indicators for Ca^{2+} based on green fluorescent proteins and calmodulin. *Nature* **388**, 882-887 (1997).
4. Miyawaki, A., Griesbeck, O., Heim, R. & Tsien, R.Y. Dynamic and quantitative Ca^{2+} measurements using improved cameleons. *Proc. Natl. Acad. Sci. USA* **96**, 2135-2140 (1999).
5. Hirose, K., Kadowaki, S., Tanabe, M., Takeshima, H. & Iino, M. Spatiotemporal dynamics of inositol 1,4,5-triphosphate that underlies complex Ca^{2+} mobilization patterns. *Science* **248**, 1527-1530 (1999).
6. Oancea, E., Teruel, M.N., Quest, A.F.G. & Meyer, T. Green fluorescent protein (GFP)-tagged cysteine-rich domains from protein kinase C as fluorescent indicators for diacylglycerol signaling in living cells. *J. Cell Biol.* **140**, 485-498 (1998).
7. Adams, S.R., Harootunian, A.T., Buechler, Y.J., Taylor, S.S. & Tsien, R.Y. Fluorescence ratio imaging of cyclic AMP in single cells. *Nature* **349**, 694-697 (1991).
8. Zaccolo, M., *et al.* A genetically encoded, fluorescent indicator for cyclic AMP in living cells. *Nat. Cell Biol.* **2**, 25-29 (1999).
9. Sato, M., Hida, N., Ozawa, T. & Umezawa, Y. Fluorescent indicators for cyclic GMP based on cyclic GMP-dependent protein kinase Iα and green fluorescent proteins. *Anal. Chem.* **72**, 5918-5924 (2000).

10. Zacharias, D.A., Baird, G.S. & Tsien, R.Y. Recent advances in technology for measuring and manipulating cell signals. *Curr. Opinion Neurobiol.* **10**, 416-421 (2000).

11. Stryer, L. Fluorescence energy transfer as a spectroscopic ruler. *Annu. Rev. Biochem.* **47**, 819-849 (1978).

12. Selvin, P.R. The renaissance of fluorescence resonance energy transfer. *Nat. Struct. Biol.* **7**, 730-734 (2000).

13. Sawyer, T.K. Src homology-2 domains: structure, mechanisms, and drug discovery. *Biopolymers* **47**, 243-261 (1998).

14. Eck, M.J., Paganon, S.D., Trub, T., Nolte, R.T. & Shoelson, S.E. Structure of the IRS-1 PTB domain bound to the juxtamembrane region of the insulin receptor. *Cell* **85**, 695-705 (1996).

15. Lu, P.J., Zhou, X.Z., Shen, M. & Lu, K.P. Function of WW Domains as phosphoserine- or phosphothreonine-binding modules. *Science* **283**, 1325-1328 (1999).

16. Bird, R.E., *et al.* Single-chain antigen-binding Proteins. *Science* **252**, 423-426 (1988).

17. Casey, J.L., Coley, A.M., Tilley, L.M. & Foley, M. Green fluorescent antibodies: novel in vitro tools. *Protein Enineering* **13**, 445-452 (2000).

18. McIlroy, B.K., Walters, J.D. & Johnson, J.D. A continuous fluorescence assay for protein kinase C. *Anal. Biochem.* **195**, 148-152 (1991).

19. Higashi, H., *et al.* Imaging of Ca^{2+}/calmodulin-dependent protein kinase II activity in hippocampal neurones. *NeuroReport* **7**, 2695-2700 (1996).

20. Higashi, H., *et al.* Imaging of cAMP-dependent protein kinase activity in living neural cells using a novel fluorescent substrate. *FEBS Lett.* **414**, 55-60 (1997).

21. Nagai, Y., *et al.* A fluorescent indicator for visualizing cAMP-induced phosphorylation in vivo. *Nat. Biotechnol.* **18**, 313-316 (2000).

22. Sun, X.J., Crimmins, D.L., Myers, M.G.Jr., Miralpeix, M. & White, M.F. Pleiotropic insulin signals are engaged by multisite phosphorylation of IRS-1. *Mol. Cell Biol.* **13**, 7418-7428 (1993).

23. Yonezawa, K., *et al.* Insulin-dependent formation of a complex containing an 85-kDa subunit of phosphatidylinositol 3-kinase and tyrosine-phosphorylated insulin receptor substrate 1. *J. Biol. Chem.* **267**, 25958-25966 (1992).

24. Hubbard, S.R. Crystal structure of the activated insulin receptor tyrosine kinase in complex with peptide substrate and ATP analog. *EMBO J.* **16**, 5573-5581 (1997).

25. Nikolic, T.R., Horn, D.J.V., Chen, D., White, M.F. & Backer, J.M. Regulation of phosphatidylinositol 3-kinase by tyrosyl phosphoproteins. *J. Biol. Chem.* **270**, 3662-3666 (1995).

26. White, M.F., Maron, R. & Kahn, C.R. Insulin rapidly stimulates tyrosine phosphorylation of a M_r-185,000 protein in intact cells. *Nature* **318**, 183-186 (1985).

27. Zhang, B., *et al.* Discovery of a small molecule insulin mimetic with antidiabetic activity in mice. *Science* **284**, 974-977 (1999).

28. Wood, H.B., *et al.* The basal SAR of a novel insulin receptor activator. *Bioorg. Med. Chem. Lett.* **10**, 1189-1192 (2000).

29. White, M.F. The insulin signaling system and the IRS proteins. *Diabetologia* **40**, S2-S17 (1997).

30. Paganon, S.D., Ottinger, E.D., Nolte, R.T., Eck, M.J. & Shoelson, S.E. Crystal structure of the pleckstrin homology-phosphotyrosine binding (PH-PTB) targeting region of insulin receptor substrate 1. *Proc. Natl. Acad. Sci. USA* **96**, 8378-8383 (1999).

31. Myers, M.G.Jr., *et al.* The pleckstrin homology domain in insulin receptor substrate-1 sensitizes insulin signaling. *J. Biol. Chem.* **270**, 11715-11718 (1995).

32. Yenush, L., *et al.* The pleckstrin homology domain is the principle link between the insulin receptor and IRS-1. *J. Biol. Chem.* **271**, 24300-24306 (1996).

33. Anai, M., *et al.* Different subcellular distribution and regulation of expression of insulin receptor substrate (IRS)-3 from those of IRS-1 and IRS-2. *J. Biol. Chem.* **273**, 29686-29692 (1998).

34. Razzini, G., *et al.* Different subcellular localization and phosphoinositides binding of insulin receptor substrate protein pleckstrin homology domains. *Mol. Endocrinol.* **14**, 823-836 (2000).

35. Myers, M.G.Jr. & White, M.F. Insulin signal transduction and the IRS proteins. *Annu. Rev. Pharmacol. Toxicol.* **36**, 615-658 (1996).

36. Zlokarnik, G., *et al.* Quantitation of transcription and clonal selection of single living cells with β-lactamase as reporter. *Science* **279**, 84-88 (1998).

37. Mere, L., *et al.* Miniaturized FRET assays and microfluidics: key components for ultra-high-throughput screening. *Drug Discovery Today* **4**, 363-369 (1999).

38. Sato, M., Ozawa, T., Yoshida, T. & Umezawa, Y. A fluorescent indicator for tyrosine phosphorylation-based insulin signaling pathways. *Anal. Chem.* **71**, 3948-3954 (1999).

39. Ng, T., *et al.* Imaging protein kinase Cα activation in cells. *Science* **283**, 2085-2089 (1999).

40. Ullman, K.S., Powers, M.A. & Forbes, D.J. Nuclear export receptors: from importin to exportin. *Cell* **90**, 967-970 (1997).

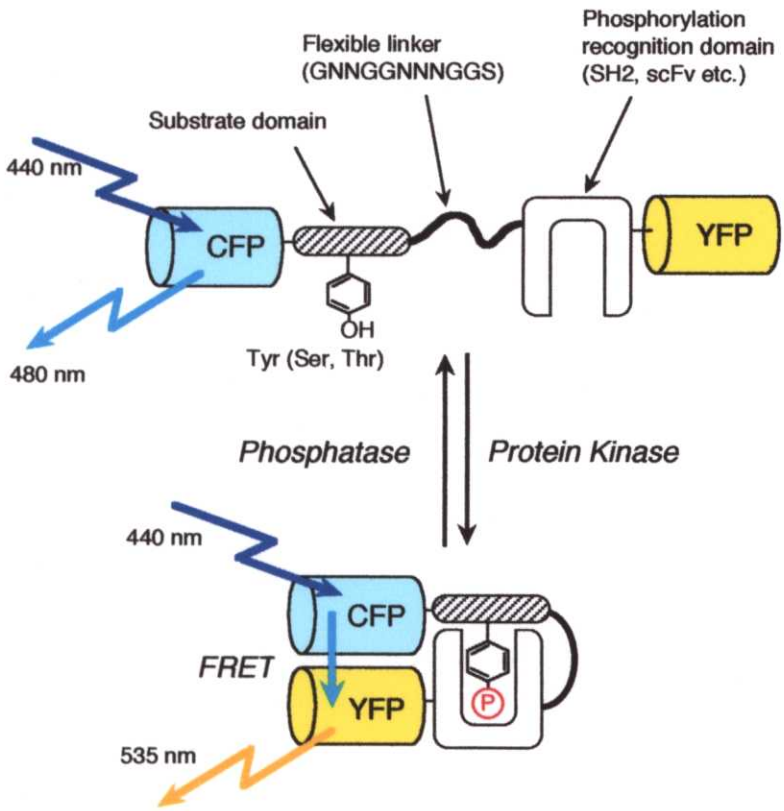

Figure 4-1. Principle of phocus for visualizing protein phosphorylation in living cells. CFP and YFP are different color mutants of green fluroescent protein (GFP) derived from *Aequorea victoria* with mammalian codons and the following additional mutations: CFP, F64L/S65T/Y66W/N146I/M153T/V163A/N212K, and YFP, S65G/V68L/Q69K/S72A/T203Y. Upon phosphorylation of the substrate domain within phocus by protein kinase, the adjacent phosphorylation recognition domain binds with the phosphorylated substrate domain, which changes the efficiency of fluorescent resonance energy transfer (FRET) between the GFP mutants within phocus.

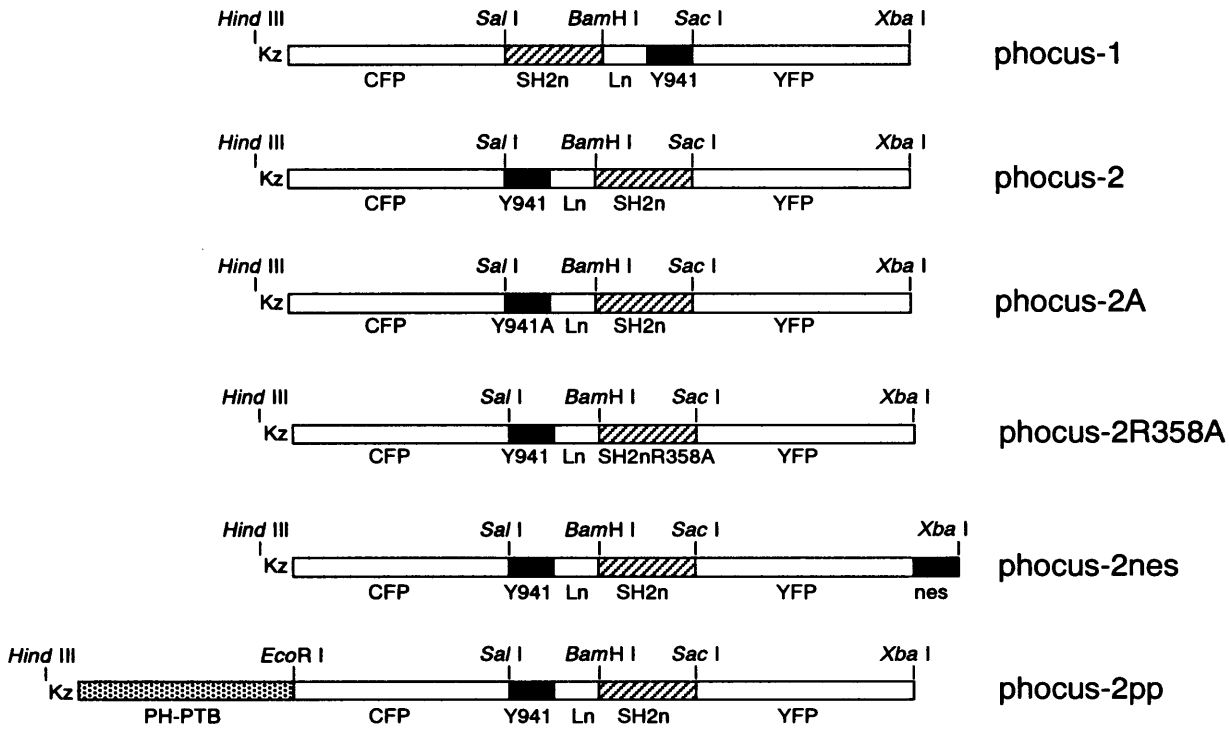

Figure 4-2. Schematic representations of domain structures of phocuses. Shown at the top of each bar are the restriction sites. Kz is an abbreviation of a Kozak sequence, which allows optimal translation initiation in mammalian cells. SH2n is an N-terminal SH2 domain from p85 subunit ($p85_{330-429}$) of bovine phosphatidylinositol 3-kinase. The amino acid sequence of Y941 is ETGTEEYMKMDLG, which is a tyrosine-phosphorylation domain by insulin receptor within IRS-1. Ln is an abbreviation of a flexible linker sequence, GNNGGNNNGGS. Nes, of which amino acid sequence is LPPLERLTL, is an abbreviation of a nuclear-export-signal sequence derived from human immunodeficiency virus protein, Rev.

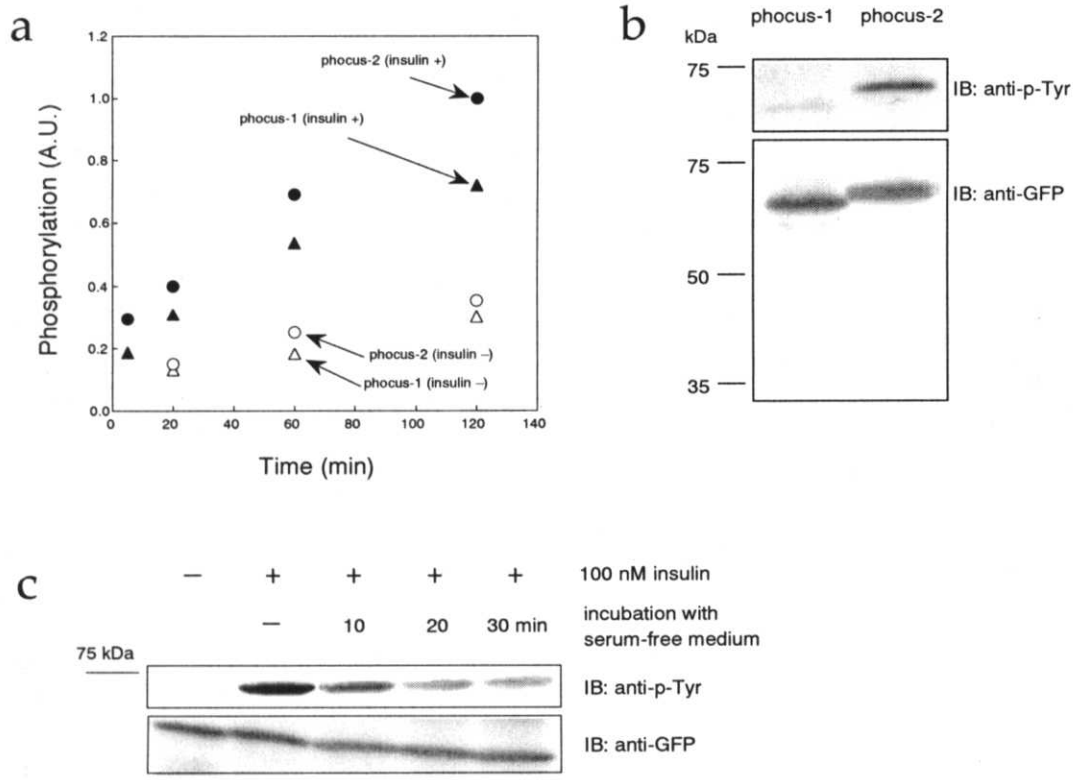

Figure 4-3. Phosphorylation and dephosphorylation of phocuses. (a) In vitro phosphorylation assay. Human insulin receptor was dissolved in a kinase buffer containing 50 mM Tris-HCl (pH 7.4), 5 mM $MnCl_2$, 50 μM ATP, 2 mM Na_3VO_4 and 0.1 % Triton X-100, with or without 100 nM insulin. The kinase reaction was initiated by adding phocus-1 or –2 purified from bacteria to give a final concentration of 5 μM. The sample solutions were incubated for 5, 20, 60 and 120 min at 37 °C. The samples were separated by SDS-polyacrylamide gel electrophoresis, and electrophoretically transferred onto a PVDF membrane. The membrane was probed with anti-phosphotyrosine antibody (PY20, 1 : 500 dilution). The obtained signal was quantified using a image analyzer (LAS-1000plus, Fujifilm). (b) In vivo phosphorylation assay. CHO-IR cells were cultured in 6-well plates and were transfected with 2 μg of each plasmid containing phocus-1 cDNA and phocus-2 cDNA. After 48 hours, the cells were serum-starved with a serum-free medium and were stimulated with 100 nM insulin for 20 min at 25 °C. The whole cell lysates were immunoprecipitated with anti-GFP antibody. Protein G-Sepharose 4FF beads were used to adsorb the immunoprecipitates and then wash four times with an ice-cold washing buffer. The samples were subjected to SDS-PAGE, and immunoblot analysis was performed with anti-phosphotyrosine antibody (PY20) and with anti-GFP antibody. No significant proteolysis of phocus-1 and –2 was observed in vivo. (c) After stimulation of phocus-2-expressing CHO-IR cells with 100 nM insulin for 5 min at 25 °C, the cells were washed, incubated in the serum-free medium at 37 °C for 10, 20 and 30 min. The whole cell lysates were immunoprecipitated with anti-GFP antibody, and immunoblot analysis was performed with anti-phosphotyrosine antibody (PY20) and with anti-GFP antibody.

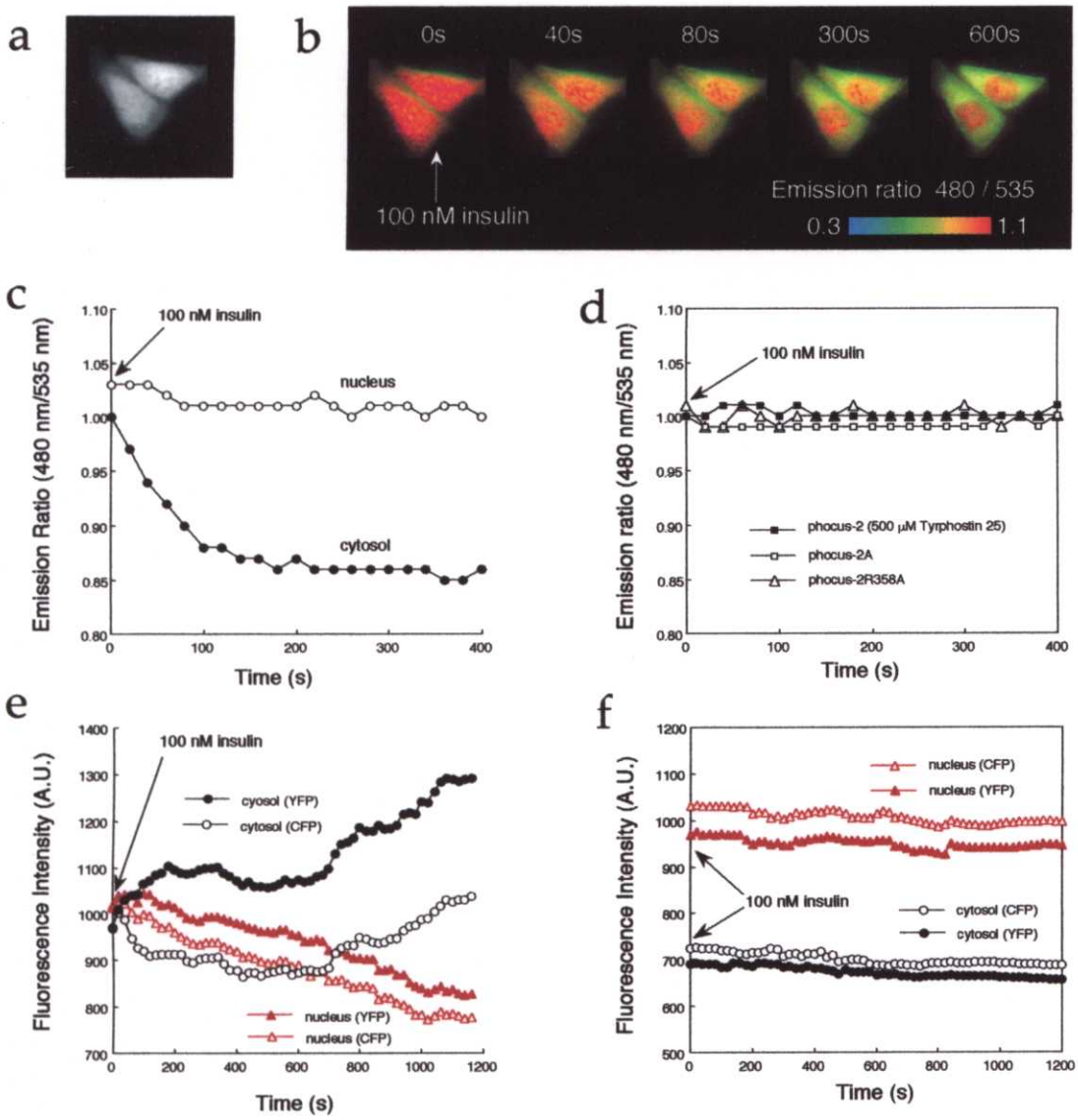

Figure 4-4. Fluorescence imaging of phocus-2 upon insulin stimulation. (a) A fluorescence image of the cell expressing phocus-2, taken using an emission filter for CFP (480 ± 15 nm), when excited at 440 nm ± 10 nm. (b) Pseudocolor images of emission ratios of 480 ± 15 nm for CFP to 535 ± 12.5 nm for YFP, when excited at 440 nm ± 10 nm, before (time 0s) and at 40, 80, 300 and 600s after the addition of 100 nM insulin at 25 °C, obtained from the CHO-IR cells expressing phocus-2. (c) Time courses of the insulin-induced CFP/YFP emission ratio obtained from Figure 4-4b in the cytosol (closed circle) and in the nucleus (open circle). (d) Time courses of the cytosolic emission ratio from phocus-2 pretreated with 500 μM tyrophostin 25 (closed square), that from phocus-2A (open square) and that from phocus-2R358A (open triangle), each when stimulated with 100 nM insulin at 25 °C. (e) Time courses of phocus-2 fluorescence at 480 ± 15 nm (nucleus; open triangle, cytosol; open circle) and 535 ± 12.5 (nucleus; closed triangle, cytosol; closed circle), each upon stimulating with 100 nM insulin at 25 °C. (f) Time courses of phocus-2A fluorescence at 480 ± 15 nm (nucleus; open triangle, cytosol; open circle) and 535 ± 12.5 (nucleus; closed triangle, cytosol; closed circle), each upon stimulating with 100 nM insulin at 25 °C. These results are from a typical experiment out of at least five independent trials.

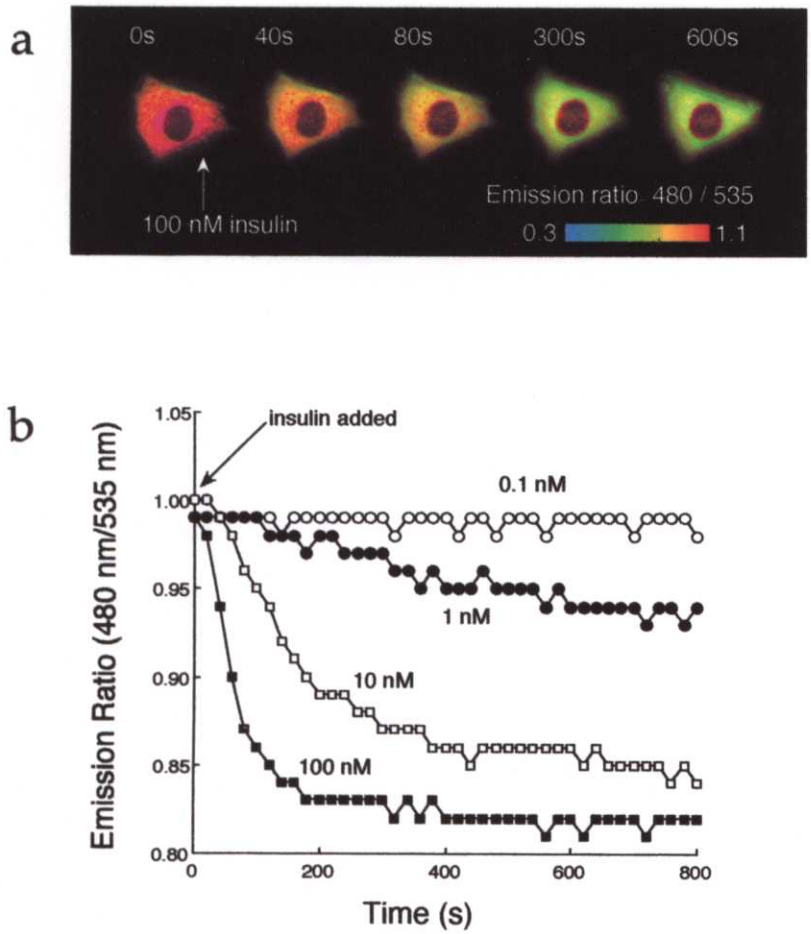

Figure 4-5. Fluorescence imaging of phocus-2nes upon insulin stimulation. (a) Pseudocolor images of the CFP/YFP emission ratios before (time 0s) and at 40, 80, 300 and 600s after the addition of 100 nM insulin, obtained from the CHO-IR cells expressing phocus-2nes. Phocus-2nes was excluded from the nucleus of CHO-IR cells due to the nuclear exporting signal sequence (nes) within phocus-2nes. (b) Response of phocus-2nes to differing concentrations of insulin in CHO-IR cells at 25 °C. These results are from a typical experiment out of at least five independent trials.

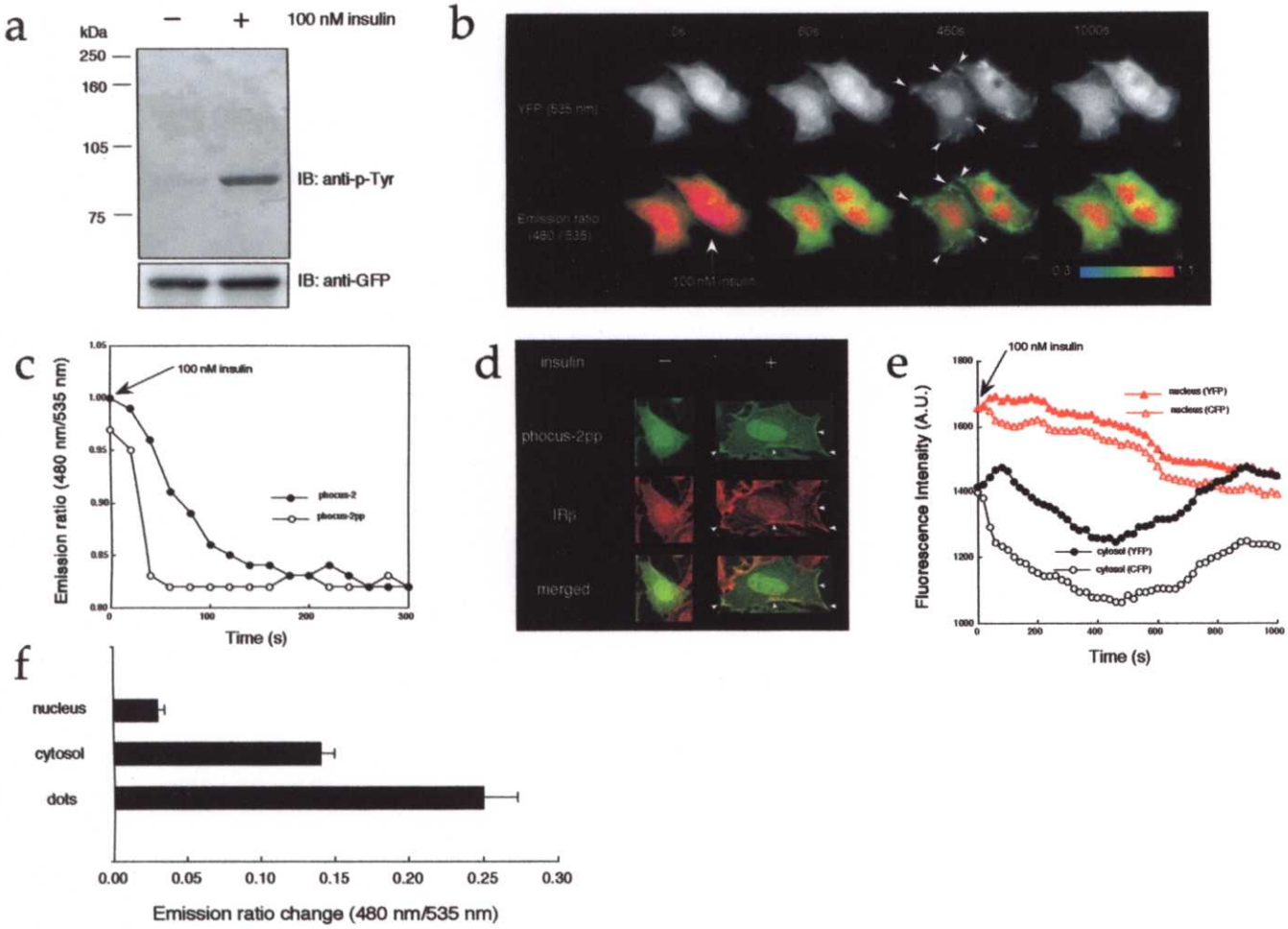

Figure 4-6. Fluorescence imaging of phocus-2pp upon insulin stimulation. (a) In vivo phosphorylation assay. CHO-IR cells expressing phocus-2pp were serum-starved with a serum-free medium and were stimulated with 100 nM insulin for 20 min at 25 °C. The whole cell lysates were immunoprecipitated with anti-GFP antibody, and immunoblot analysis was performed with anti-phosphotyrosine antibody (PY20) and with anti-GFP antibody. (b) Fluorescence images at 535 ± 12.5 nm for YFP and pseudocolor images of emission ratios of 480 ± 15 nm for CFP to 535 ± 12.5 nm for YFP, when excited at 440 nm ± 10 nm, before (time 0s) and at 60, 460 and 1000s after the addition of 100 nM insulin at 25 °C, obtained from the CHO-IR cells expressing phocus-2pp. Insulin-induced localization of phocus-2pp at the plasma membrane is indicated by white arrows in the image at 460s. (c) Time course of the cytosolic emission ratio for phocus-2pp (open circle) was compared with that for phocus-2 (closed circle), each when stimulated with 100 nM insulin at 25 °C. (d) Subcellular localization of phocus-2pp and insulin receptor (white arrow heads), when stimulated with 100 nM insulin for 7 min at 25 °C. After insulin stimulation, cells on the glass coverslips were fixed and stained with rabbit antibody against β-subunit of insulin receptor (IRβ). The cells were further stained with anti-rabbit IgG antibody labeled with Cy5. The coverslips were mounted onto the slide and observed with a confocal laser scanning microscope (LSM 510, Carl Zeiss) at 488 nm and 633 nm excitation for phocus-2pp and IRβ (Cy5), respectively. (e) Time courses of phocus-2pp fluorescence at 480 ± 15 nm (nucleus; open triangle, cytosol; open circle) and 535 ± 12.5 (nucleus; closed triangle, cytosol; closed circle), each upon stimulating with 100 nM insulin at 25 °C. (f) A comparison of the changes in CFP/YFP emission ratio in the nucleus, cytosol and dot-like structures of CHO-IR cells expressing phocus-2pp, after 460 seconds of insulin stimulation. The results are the means and standard deviations of three separate.

Chapter 5.

General Conclusion

To visualize molecular events for cGMP- and protein phosphorylation-based signaling in living cells, I developed novel fluorescent indicators and discussed their applicability for fluorescence imaging and for high-throughput screening of pharmaceuticals from thousands of candidate chemicals. All of the indicators thus developed depended upon analyte-induced alternations in fluorescence resonance energy transfer (FRET) between two different color fluorophores. Fluorescence ratio imaging of FRET, with which fluorescence intensity variations due to indicator concentrations, optical path lengths and excitation intensities were canceled out, caused stable measurements of the molecular events within single live cells.

Using fluorescent indicators for cGMP, CGYs, I have demonstrated that nitric oxide (NO)-induced cellular accumulation of cGMP was not necessarily in parallel with NO concentration, and have found an oscillating dynamics of cGMP concentration in single living cells.

Fluorescent indicators for protein phosphorylation-based signal transduction, FRET pair and phocuses, were exemplified using insulin signaling proteins, with which protein phosphorylation by insulin receptor was visualized. For general applicability, the endogenous phosphorylation-recognition domain within the present indicators could be replaced with single chain antibodies (scFvs)[1, 2] against the phosphorylated substrate sequences of interest. Not only protein

phosphorylation but also other mechanism for signal transduction, such as protein acetylation[3, 4] is our next target for improving the present fluorescent indicator.

Further perspective

Although not included in this thesis, I have found that FRET is powerful not only for developing the fluorescent indicators for second messengers and protein-phosphorylation but also for visualizing protein functional dynamics coupled with the translocation of signaling proteins. Concerning with protein-based signaling, green fluorescent protein (GFP) have been extensively used for labeling the signaling proteins including protein kinases to visualize the fusion proteins of GFP and the signaling proteins of interest[5, 6]. For instance, on the basis of this approach, protein kinase C (PKC) was found to translocate to the plasma membrane in response to agonist stimulation and the following cellular accumulation of second messengers such as Ca^{2+}, diacylglycerol and phosphatidylinositol-3,4,5-triphosphate[7-9]. However, it has been unclear where PKC is activated and where the activated PKC goes within living cells. To overcome this limitation, I labeled PKC with two different color GFPs, as donor and acceptor for FRET, to both ends of PKC. Using this fusion protein, I could visualize an agonist-induced conformational change in PKC, which is a measure for PKC activation, together with its subcellular localization. This exemplifies that the FRET approach for signaling protein, not conventional approach using only one fluorophore such as GFP, enables to add functional information, i.e. activation of the signaling protein based on its conformational change, to spatial information within cells. Fluorescence imaging with the "molecular spies" thus created should contribute to understand the spatial and temporal dynamics of signal transduction within cells, tissues and organs.

References

1. Bird, R.E., *et al.* Single-chain antigen-binding Proteins. *Science* **252**, 423-426 (1988).
2. Casey, J.L., Coley, A.M., Tilley, L.M. & Foley, M. Green fluorescent antibodies: novel in vitro tools. *Protein Enineering* **13**, 445-452 (2000).
3. Vogelauer, M., Wu, J., Suka, N. & Grunstein, M. Global histone acetylation and deacetylation in yeast. *Nature* **408**, 495-498 (2000).
4. Luo, J., Su, F., Chen, D., Shiloh, A. & Gu, W. Deacetylation of p53 modulates its effect on cell growth and apoptosis. *Nature* **408**, 377-381 (2000).
5. Chalfie, M. & Kain, S. *Green fluorescent protein: properties, applications, and protocols* (Willey-Liss, 1997).
6. Tsien, R.Y. The green fluorescent protein. *Annu. Rev. Biochem* **67**, 509-544 (1998).
7. Sakai, N., *et al.* Direct visualization of the translocation of the γ-subspecies of protein kinase C in living cells using fusion proteins with green fluorescent protein. *J. Cell Biol.* **139**, 1465-1476 (1997).
8. Feng, X., *et al.* Visualization of dynamic trafficking of a protein kinase C βII/green fluorescent protein conjugate reveals differences in G protein-coupled receptor activation and desensitization. *J. Biol. Chem.* **273**, 10755-10762 (1998).
9. Oancea, E. & Meyer, T. Protien kinase C as a molecular machine for decoding calcium and diacylglycarol signals. *Cell* **95**, 307-318 (1998).